USING A 3D FINITE ELEMENT FORWARD MODELING CODE TO ANALYZE RESISTIVE STRUCTURES WITH CONTROLLED-SOURCE ELECTROMAGNETICS IN A MARINE ENVIRONMENT

A Thesis

by

JOSHUA DAVID KING

Submitted to the Office of Graduate Studies of
Texas A&M University
in partial fulfillment of the requirements for the degree of

MASTER OF SCIENCE

December 2004

Major Subject: Geophysics

USING A 3D FINITE ELEMENT FORWARD MODELING CODE TO ANALYZE RESISTIVE STRUCTURES WITH CONTROLLED-SOURCE ELECTROMAGNETICS IN A MARINE ENVIRONMENT

A Thesis

by

JOSHUA DAVID KING

Submitted to Texas A&M University in
partial fulfillment of the requirements for the
degree of

MASTER OF SCIENCE

Approved as to style and content by:

Mark E. Everett (Chair of Committee)	William Bryant (Member)
David Sparks (Member)	Roger Sassen (Member)

Richard Carlson
(Head of Department)

December 2004

Major Subject: Geophysics

ABSTRACT

Using a 3D Finite Element Forward Modeling Code to Analyze Resistive Structures with Controlled-Source Electromagnetics in a Marine Environment. (December 2004)

Joshua David King, B.S., Keene State College

Chair of Advisory Committee: Dr. Mark E. Everett

Controlled-Source Electromagnetics (CSEM) is a method that has been used since the 1980's in the marine environment for determining electrical properties of the subsurface. Receivers on the seafloor collect total electric and magnetic fields which are produced as a result of interaction of the transmitter generated primary fields with the seawater and subsurface.

Badea *et al*. (2001) coded an existing algorithm for solving Maxwell's equations. This finite element 3D forward modeling algorithm is used to simulate CSEM experiments. The objective of the present study is to model the changes in electromagnetic response for a resistive disk and a more geometrically complex structure, which are rough approximations of hydrocarbon reservoirs. The parameters that are varied in studying these subsurface structures are the disk radius, disk depth, the transmitter frequency, the transmitter location, and the structure orientation.

The results showed that a disk of finite radius behaves similar to an infinite disk at short range and grades into double half-space behavior at longer ranges. The frequency of the transmitter must be tuned to the disk depth as certain frequencies will penetrate too shallow or too deep to probe the disk. Moving the transmitter away from the receivers

causes a decrease in signal strength, but exhibits a greater capacity to distinguish between the double half-space and infinite disk scenarios.

The disk was then replaced by a more complex structure. To determine if the 3D nature of the structure may be located a study was undertaken to probe the structure from different perspectives using different transmitter locations and azimuths. It is determined that the 3D nature of the structure could not be observed until the structure's thickness is sufficiently large.

The goal of the study is to better understand the effect of subsurface parameters on the total fields and show the usefulness of the 3D forward modeling code. Understanding the relationships between these parameters and the resulting signals is important in terms of setting up a real experiment. Marine CSEM studies are costly and using a valuable tool such as an accurate finite element 3D forward modeling algorithm may save time and money.

ACKNOWLEDGEMENTS

I would like to thank Mark Everett for taking the time to answer all of my questions and for guidance on many subjects. I owe my thanks to Alfonso Benavides for helping me understand electromagnetics in all of its glory. I would also like to thank Jamie Collins and Zach Long for help with this project. I would like to thank Katherine Kilday for being there through the whole process with support. Lastly, I would like to thank my parents Beverly and David King for support given to me while working on this project.

TABLE OF CONTENTS

1. INTRODUCTION

1.1 Previous Studies

The use of electromagnetics in the marine environment has been studied for about two decades. The two methods used have been the passive magnetotellurics (MT) method and the active controlled-source method. Studies have used MT to look at mid-ocean ridge environments and as a tool for petroleum exploration. CSEM has also been used for the study of ridge environments and more recently for petroleum exploration.

Marine electromagnetics has several advantages in areas where seismic has difficulty in obtaining good quality data. In environments including salt bodies, carbonates, or volcanics, seismic has been shown to produce poor results because of scattering of the signal. Even the most advanced 3-D seismic methods may fail in these settings (Hoversten *et al.*, 1998). Such environments bode well for electromagnetics because these bodies have resistivities which vary greatly from those of the surrounding sediments. However electromagnetics is sensitive to bulk properties such as porosity and not to sharp boundaries, which are more of a seismic target. Therefore, these two methods (electromagnetic and seismic) should produce best results when used together because they provide complementary information (Hoversten *et al.*, 1998)

MT takes advantage of naturally occurring electromagnetic fields to estimate the electrical properties of subsurface structure. In the marine environment, high frequency signal components (roughly above 0.01 Hz) are attenuated as they propagate through the seawater, leaving only the long frequency components with an appreciable amplitude.

This thesis follows the style of *Geophysical Journal International.*

This natural selection of frequencies allows for deep, albeit low-resolution studies. For this reason, MT has been mostly used for deep crustal studies in the past. It was not until Constable *et al*. (1998) designed a MT receiver (RX) which amplified the weak higher frequencies, in the period range 3s to 1000s, that a new research area opened for the method. MT may now be used for shallow crustal studies and as an additional tool for petroleum studies.

The use of MT as a shallow marine investigative tool was emphasized by Hoversten *et al.* (1998). Forward modeling results of a salt body were inverted to show that the base of salt could be defined. This was done most successfully when pre-defined boundaries from the seismic results were used in conjunction with the MT (Hoversten *et al.*, 1998). The next step was to field test the equipment.

A study was done by Hoversten *et al*. (2000) at the Gemini site in the Gulf of Mexico. This site was chosen because the location of base of salt was considered to be well-determined and an accurate comparison to previous seismic imaging was possible. It was shown that MT may be used to accurately model the base of the salt body; suggesting its usefulness to offshore petroleum exploration, because seismic had difficulty imaging base of salt.

CSEM differs from MT in that the signal used is generated by a controlled transmitter (TX) located on or near the seafloor. The proximity of the source to the seafloor allows for the use of shorter frequencies which in MT would otherwise have been attenuated by the depth of the water column. These introduced frequencies result in higher resolution of the shallow geology (up to several kilometers in depth). This method, like MT, is useful in mapping porosity. A system was developed and used

successfully to map near-surface porosity in coastal areas (Cheesman *et al.* 1990; Cheesman *et al*. 1993). CSEM also has been used to study mid-ocean ridges and other marine environments. Hydrothermal mounds have been studied with CSEM methods (Nobes *et al.* 1992; Evans and Everett 1994; Cairns *et al*. 1996). Several surveys gathered data from these environments and used inverse modeling to study the structure of the ridge (Young and Cox 1981; Cox *et al.* 1986; Evans *et al*. 1991; Evans *et al.* 1994; Constable and Cox 1996; MacGregor *et al.* 1998; Sinha *et al*. 1998; and MacGregor *et al.* 2001). Some of these studies, as well as others, used forward modeling to provide understanding of the EM responses from typical geology (Evans *et al.* 1991; Evans and Everett 1994; Flosadottir and Constable 1996, MacGregor *et al.* 2001; Unsworth 1994). Flosadottir and Constable (1996) also used forward modeling for experiment design. The problem of 2.5D forward modeling has been solved and used to aid in interpretation and improve experimental design (Unsworth *et al.* 1993; Everett and Edwards 1992). The 2.5D forward modeling code models the use of a 3D source over a 2D structure. None of these studies however, have employed a fully 3D forward modeling code which entails a 3D source used over a 3D structure.

Until now there have been no papers written on the subject of 3D controlled-source electromagnetic forward modeling for its use in marine petroleum exploration. The intent of this study is to analyze CSEM frequency domain responses of resistive disks and a more complex structure which are rough representations of offshore hydrocarbon reservoirs. This is done to simulate a marine CSEM experiment and also to assess the utility of the 3D forward code.

1.2 Controlled-Source Electromagnetics

The marine controlled-source electromagnetic method involves setting out receivers on the seafloor which read signals from a transmitter towed behind and powered from a ship (Figure 1). The power source onboard the ship generates an alternating current which is sent down the cable to the transmitter. The current is dropped down in voltage and runs through the transmitter, which in this case is a horizontal dipole of ~ 100 m in length. A magnetic field is generated by the time-dependent current. This magnetic field diffuses outwards through both the seawater and seafloor. As the magnetic field passes through materials of various resistivities it will generate secondary electric currents which in turn generate magnetic fields that are read by the seafloor receivers previously placed on the seafloor. These data are analyzed to interpret the resistive structure of the seafloor between the transmitter and the receivers.

The desired information is encoded in the fields propagating through the seafloor. The seawater will also generate these secondary electric currents and magnetic fields but these are typically used only to calibrate the apparatus since they encode known information about seawater. The spatial decay of the fields can be characterized by the skin depth equation:

$$d_s = \frac{500}{\sqrt{\sigma f}};$$

where σ represents the conductivity of the medium in S/m, f is the transmitter frequency in Hz, and d_s is measured in m. Fortunately the seawater has a smaller skin depth than the seafloor, so signals attenuate more rapidly in seawater and are read only by receivers in close proximity to the transmitter. Further receivers read only the interesting seafloor signals. The data from the received signals contains a vast and complicated amount of

resistivity information about the intervening material between transmitter and receiver, thus making interpretation difficult at best. This is where forward modeling can enter the picture, i.e. to help understand the experimental data. In forward modeling, computational limitations dictate that only highly idealized models of actual geological resistivity distributions can be evaluated. The idealizations should however contain sufficient detail to model first-order response variations of actual structures.

1.3 3D Finite Element Code

1.3.1 General Overview of the Code

The 3D forward modeling code used in this study is a finite element algorithm developed by Mark Everett of Texas A&M University and Eugene Badea formerly of Haliburton, Inc. The code has been used in the past for modeling electromagnetic well logging in petroleum exploration (Badea *et al.*, 2001). This code has been validated for 1D, 2D and 3D structures and solves the governing Maxwells equations as formulated in terms of Coulomb gauged potentials. The forward problem is formulated in cylindrical coordinates.

The finite element algorithm generates a cylindrical mesh formed from about 1000s of interconnected nodes. A wide range of geological structures may be modeled since many mesh parameters (such as the node distribution) can be altered. A desired structure or environment may be created by assigning elements various conductivities based on the cylindrical coordinates of their constituent nodes. Once this is done, the next step is usually to define the location of the transmitter with an external file which

controls parameters of the mesh. The code can then be run as a double half-space with a uniform or a heterogeneous lower half-space representing the seafloor conductivity (Figure 1). The code also permits the introduction of seafloor bathymetry, if required.

As the final result, after the finite element matrix system has been solved, each node has its own value for the electric field and magnetic field. Every node can therefore be visualized as a point receiver. The desired nodes must then be selected which would represent experimental receiver locations. In this particular study some of the nodes on the seafloor are representative of receivers. In localized areas where rapid changes occur in the response, the mesh can be refined to better capture the true signature of the response.

Local mesh refinement may be a very useful tool, especially for small TX-RX offsets. The user refines a region by defining its boundaries, i.e. selecting the desired radius, depth range, and azimuth desired. The tetrahedra in the refinement region are subdivided dependent upon the level of refinement selected. New nodes are created, which can be considered to be adding additional receivers to obtain a higher resolution. A more complete description of the refinement process can be found in Badea *et al*. (2001).

1.3.2 General Description of the Math

Until recently finite difference (FD) methods were used to solve Maxwell's diffusion equations for heterogeneous media. A limiting factor of FD methods is that a structured mesh is required. A second method, finite element (FE), allows for unstructured mesh designs which are more flexible in terms of geometry and hence more

useful for modeling complicated geological variability. It is conventionally thought that FE solvers demand overwhelming computational power; however a rapid increase in computational technology has allowed for the desktop use of FE modeling. Badea *et al.* (2001) used FE methods with Coulomb gauged electromagnetic (EM) potentials to solve Maxwell's diffusion equations.

Badea *et al.* (2001) formulated their FE solutions in terms of coupled vector-scalar potentials ($\mathbf{A}, \Psi$) where **A** is the magnetic vector potential and Ψ is the electric scalar potential. Accordingly the formulation has to satisfy two requirements: the normal electric field is allowed to jump at interfaces while the tangential component must be continuous and there must be no divergent or spurious modes in the EM fields. Badea *et al.* (2001) used the vector/scalar approach because the vector magnetic potential, **A**, and the electric scalar potential, Ψ, are continuous at the interfaces ensuring the first requirement. The Coulomb gauge condition of $\nabla \cdot \mathrm{A} = 0$ ensures the second requirement, that there are no divergent modes in the calculated EM fields.

The following is a simplified version of the mathematical development found in Badea *et al.* (2001). Maxwell's diffusion equations are valid only for the low frequencies (such that $\sigma << \varepsilon\omega$, where σ represents electrical conductivity, ε represents electric permittivity, and ω represents angular frequency) used in CSEM. The basic equations are

$$\nabla \times \mathbf{E} = i\omega\mu_0 \mathbf{H}; \tag{1}$$

$$\nabla \times \mathbf{H} = \mathbf{J} = \mathbf{J}_s + \sigma \mathbf{E}. \tag{2}$$

The symbol μ_0 is the magnetic permeability, $\mathbf{J}_s$ is the electric current density of the source, and σ equals the electrical conductivity. Badea *et al.* (2001) apply the equation

$\mathbf{B} = \mu_0\mathbf{H}$ to relate the magnetic induction and magnetic field vectors and the divergence free conditions $\nabla \cdot \mathbf{J} = 0$ and $\nabla \cdot \mathbf{B} = 0$ to ensure there are no sources or sinks of current and magnetic field, respectively, in the solution.

To increase ease of solving Badea *et al.* (2001) write **E** and **H** in terms of **A** and Ψ, as follows:

$$\mathbf{B} \equiv \nabla \times \mathbf{A}; \tag{3}$$

$$\mathbf{E} \equiv i\omega\mathbf{A} + \nabla\Psi \ . \tag{4}$$

Equation (2) becomes:

$$\nabla \times \nabla \times \mathbf{A} = \mu_0\mathbf{J}_s + i\omega\mu_0\sigma(\mathbf{A} + \nabla\Psi). \tag{5}$$

Badea *et al.* (2001) then use a method proposed by Biro and Preis (1989) incorporating the term $-\nabla(\nabla \cdot \mathbf{A})$ to the left side of equation (5) to avoid asymmetric FE matrices. These matrices could result in numerically unstable modes. The result is

$$\nabla \times \nabla \times \mathbf{A} - \nabla(\nabla \cdot \mathbf{A}) - i\omega\mu_0\sigma(\mathbf{A} + \nabla\Psi) = \mu_0\mathbf{J}_s. \tag{6}$$

The added term $-\nabla(\nabla \cdot \mathbf{A})$ disappears leaving the equation unchanged if $\nabla \cdot \mathbf{A} = 0$ is satisfied. A vector identity $\nabla \times \nabla \times \mathbf{A} - \nabla(\nabla \cdot \mathbf{A}) = -\nabla^2\mathbf{A}$ is applied by the authors, showing that equation (6) is equivalent to a Helmholtz equation.

$$\nabla\mathbf{A}^2 + i\omega\mu_0\sigma(\mathbf{A} + \nabla\Psi) = -\mu_0\mathbf{J}_s \tag{7}$$

The authors then take the divergence of equation (5) to show that the divergence-free condition $\nabla \cdot \mathbf{J} = 0$ is automatically enforced. Since equation (5) was altered (7) by itself cannot be used to guarantee divergence free current density. To enforce $\nabla \cdot \mathbf{J} = 0$, Badea *et al.* (2001) augment (7) with the following equation

$$\nabla \cdot [i\omega\mu_0\sigma(\mathbf{A} + \nabla\Psi)] = 0. \tag{8}$$

The authors used a secondary potential formulation to model EM induction. This allowed them to introduce the source in terms of primary EM potentials ($\mathbf{A_p}$, Ψ_p). The primary potentials ($\mathbf{A_p}$, Ψ_p) are known solutions to a problem with conductivity σ_p. The secondary potentials ($\mathbf{A_s}$, Ψ_s) are defined by $\mathbf{A} = \mathbf{A_p} + \mathbf{A_s}$ and $\Psi = \Psi_p + \Psi_s$. The governing equations (7 and 8) now become:

$$\nabla^2\mathbf{A}_s + i\omega\mu_0\sigma(\mathbf{A}_s + \nabla\Psi_s) = -i\omega\mu_0\Delta\sigma(\mathbf{A}_p + \nabla\Psi_p)\,; \tag{9}$$

$$\nabla\cdot\,[i\omega\mu_0\sigma(\mathbf{A}_s + \nabla\Psi_s)] = -\nabla\cdot\,[i\omega\mu_0\Delta\sigma(\mathbf{A}_p + \nabla\Psi_p)]\,, \tag{10}$$

where $\Delta\sigma = \sigma - \sigma_p$ is the difference between the conductivity distribution (σ) whose response is required and the background distribution (σ_p) whose response is known. Equations (9 and 10) will be the governing equations for providing the electric and magnetic field solutions.

2. METHODS

This study consists of forward modeling the EM response from a marine geological formation with embedded resistive structures. The transmitter location is varied as well as the conductivities and geometries of the subsurface resistivity structure. A primary goal is to understand how the signals received relate to the embedded subsurface structures. Another goal is to produce simulated responses which can be used to better understand experimental data and possibly to improve survey and equipment design.

2.1 1D vs. 3D – Validating the 3D Finite Element Algorithm

The first step is to validate the 3D finite element algorithm with an analytic code. A double half-space model is used for the comparison. The 1D code solves for a transmitter 100 m above the homogeneous seafloor. This is compared to the results of the 3D finite element algorithm with a transmitter located 100 m above the seafloor ($z = 0$) at the zero location ($x = 0$, $y = 0$). Both codes are run for short and long transmitter-receiver offsets relative to the skin depth. The mesh boundary for the short TX-RX offset is 1000 m and the mesh boundary for the long TX-RX offset is 10 km. The top and bottom of the mesh are located at -1500 m and 1500 m respectively.

2.2 Resistive Disk

The basic design of the mesh conforms to a double half-space with the upper homogeneous half representing the seawater and the lower heterogeneous half-space representing the sub-seafloor sediments. A finite water column thickness (e g air wave)

is neglected by assuming infinite water depth. The mesh top and bottom are still located at -1500 m and 1500 m respectively, but the maximum radius is now 20 km. These parameters will not be changed again. The first embedded seafloor structure to be examined is a simple disk (Figure 2). The parameters that are varied include the transmitter frequency, the disk radius, thickness, and burial depth in the subsurface sediments. The structure (disk) is located in the lower half of a homogeneous double half-space. The disk is intended to idealize the complicated geometry of a hydrocarbon reservoir. The conductivities selected are chosen to represent those of actual seafloor sediments containing hydrocarbons and were suggested by Steve Constable of Scripps Institute of Oceanography. The conductivities of these bodies may be varied to represent various sediment or rock types, as required.

An important fact to keep in mind throughout all modeling is that the same receiver locations will be used. These are the nodes from 0 m to 20 km along the x-axis (y = 0, z = 0). Each of the next sections will focus on one of the various parameters that were studied.

2.2.1 Disk Frequency and Radii

The first parameters studied are the disk radius and transmitter frequency. The disk is placed at a burial depth of 525 m with its center at x = 0 and y = 0. The disk has radial symmetry and is ~38 m in thickness. The transmitter location is on the x-axis at -1000 m. This location is chosen because the seawater signals, which are undesired noise, should have attenuated significantly by this distance. The transmitter is located at 100 m (z = -100 m) above the seafloor. The transmitter frequency range used is from

0.005 to 1.0 Hz. The models run consisted of a double half-space containing no disk (double half-space); a 1250 m disk; 2500 m disk; 5000 m disk; and an essentially infinite disk (20 km disk). The disk radii are chosen to represent the size of actual hydrocarbon reservoirs of interest to marine CSEM explorationists.

The double half-space scenario and the infinite disk scenario represent the two end-member responses while the finite-disk responses should fall in between. At short TX-RX range the finite disks should behave like an infinite disk, but grade into double half-space behavior at long range. Once the effects of this parameter on the total electric field are satisfactorily understood the next step is to move the location of the transmitter.

2.2.2 Transmitter Location

A series of transmitter locations are run from 0 m to -5000 m along the x-axis. All of the other parameters listed in the previous section are used including the various disk radii scenarios. The purpose of this experiment is to recreate, very roughly, the towing of the transmitter along the seafloor. The idea is that each transmitter location is a snapshot along the towline. This is done to see if the total electric field results will behave in a predictable manner. The fields read by the receivers (which are always at 0 m to 20 km along the x-axis) should decrease in signal strength as the transmitter position moves away. Insight into the separation of the response curves for the different modeled disk radii in this way can be gained. Once these predictions are confirmed and the separation of the disk curves understood, the disk depth is the next parameter altered.

2.2.3 Disk Depth

Three disk depths: 225 m; 525 m; and 1012.5 m are selected which are sufficiently separated from each other and conform to the pre-designed mesh boundaries. The double half-space, finite disk, and infinite disk scenarios are used, a frequency of 0.1 Hz is also used, and a transmitter location of -1000 m on the x-axis is chosen. The main objective of this set of numerical simulations is to determine how the TX-RX separation affects the response for various disk depths. This parameter concludes the experiments done on the disk; the next numerical experiments involve a change in the geometry of the disk.

2.3 Disk Thickness

Before the complex structure is introduced a three-layered disk is studied as a intermediate case between the single-layered disk and the complex structure. The 3-layered disk is three times the thickness of the single-layered disk, or ~ 112 m thick. The top of the three-layered disk is located at the same 525 m burial depth as that of the single-layered disk. The disk radii scenarios included the double half-space, 1250 m disk, 2500 m disk, 5000 m disk, and an infinite three-layered disk. The parameter that is altered in this model is the frequency. The main objective here is to analyze which frequency is the most appropriate for detailed imaging of the three-layered disk. This is decided by determining which frequency resulted in the greatest separation between the double-half-space response curve and the infinite disk response curve. No further work is done with this particular disk geometry and the complex geometric structure is studied next.

2.4 Complex Structure

The next step is to introduce a more complex structure. The structure used is suggested by Steve Constable of Scripps Institute of Oceanography and is based on experience using marine EM for offshore exploration (Fig. 3). This structure is designed to be a more geometrically accurate representation of a hydrocarbon reservoir than the disk yet it still conforms to the underlying cylindrical geometry of the mesh. The structure is three-tiered with the bottom layer being a full disk with the largest diameter (3750 m), the second layer above is a $\Delta\phi = \frac{3\pi}{2}$ radian (¾ of a full 2π radians circle) circle with a smaller radius, and finally an annulus segment, with an azimuthal radius of $\Delta\phi = \frac{\pi}{2}$ radians (¼ of a full 2π radian circle), located on top (Figure 3). The parameters varied are the transmitter location, transmitter frequency, the structure orientation, and the thickness of the structure. The geometry of the structure is not varied as this is a specific design.

The main objective of studying this structure is to understand the effect of structure geometry on CSEM responses. A second objective is to examine the CSEM responses to try to locate the thickest part of the structure where a well would be drilled. Locating this "sweet spot" is done by using several transmitter locations around the structure and comparing responses of receivers in a profile across the structure. Subtle changes in the horizontal total electric field are related to the known location of the sweet spot to determine whether and how these changes are indicative of this location

2.4.1 Transmitter Frequency

The first objective is to determine which frequency is best to study the structure. This is done by selecting the frequency which produces the greatest and most consistent separation between the double half-space response curves and those of the structure. It is of interest to determine whether a different frequency is more useful in imaging this structure as compared to the best frequency for the single or triple-layered disk. The structure is buried at 225 m and 525 m.

2.4.2 Structure Depth

The final experimental trial is to alter the depth of the structure. The same burial depths of 225 m, 525 m, and 1012.5 m from the previous experiments are used. These models are run to look for differences in the strength of the curves between those of the structure and those of the single and triple-layered disks.

2.4.3 Structure Orientation

The geometry of this structure is not altered; however the transmitter is moved to locations around the structure to view it from different perspectives. One problem with this is that the 3D code was temporarily designed to use receivers in a line along the x-axis. Instead of moving the TX, the structure is turned so that the open circle is facing towards the negative x-axis and also the positive side of the x-axis. Although the code could have been modified, an easier solution is to rotate the structure and leave the transmitter in the same location of -1000 m on the x-axis. This simulates a perpendicular tow across the broad-side of the structure. The last measure is to imitate the transmitter

on the y-axis by rotating the structure so that its open face is aligned with the y-axis. This modeling experiment is done for burial depths of 225 m and 525 m. This concludes transmitter location scenarios.

The objective of this section of experiments is to find if there is a difference in response between the three different orientations that may indicate the location of the shallow portion of the structure. In an actual experiment, for example, it is useful to know how to best combine endfire and broadside TX tow responses in order to isolate the sweet spot.

2.4.4 Structure Thickness

The final modeling is done to explore the changes in EM response caused by thickening the structure. The structure has already been tested for a thickness of ~112 m in all orientations (facing the negative x-axis, positive x-axis, and the positive y-axis). The same models are run again at all transmitter positions and structure orientations for structure thicknesses of ~ 336 m and 675 m. The model runs are done at a depth of 525 m, with a TX frequency of 0.1 Hz and a TX location of -1000 m on the x-axis. This section concludes the methods.

3. RESULTS

3.1 1D vs. 3D – Validating the 3D Finite Element Algorithm

The 3D finite element code is compared to the 1D analytic code. The first trials for a frequency of 1.0 Hz, seawater conductivity 3.0 S/m and seafloor conductivity 1.0 S/m are run for short TX-RX offsets (from 0-1000 m). Four levels of refinement are necessary to obtain an accurate match in the response (Table 1). The results show an increasingly accurate match with the 1D analytic response as the mesh is refined (Fig. 4). The figure indicates that local refinement is required to match the short offset receiver analytic response. The next step is to model a much longer TX-RX offset (from 0-10 km).

Long offsets are common in actual experiments where the ranges can be in excess of 10 km. The long offset results proved to be less accurate even when including the four local refinements (Fig. 5). Long offset total electric fields fell off more quickly with the 1D algorithm than with the 3D algorithm. As the analytic code has been well-tested to provide accurate responses, changes had to be made to the 3D code. Through trial and error it is found that the finite-element algorithm is very sensitive to the location of the top and bottom of the mesh. However, a better match with the 1D algorithm is not obtained for these models no matter how the geometry of the mesh was altered.

The original parameters used for the frequency and the conductivities are changed. It is found again through running the code many times and comparing the results to the 1D results that a product of the seafloor conductivity and frequency of order one or greater ($\sigma\omega > 1 \ \frac{\text{Sgrad}}{\text{mgs}}$) results in an inaccurate match. The decision is made to

keep the conductivities as close to the original value of σ =1.0 S/m while lowering the frequency to obtain more accurate results. The reason for this is that real world experiments would alter the frequency as the geologic conductivities cannot be altered.

Reasonable results are obtained for short TX-RX offset (Fig. 6) and long TX-RX offset (Fig. 7) when the frequency was lowered to 0.1 Hz from 1.0 Hz while the mesh size is shortened and widened. The ratio of height (z) to width (x and y) of the mesh is about 1:3.3 respectively. The results for these runs of the 3D finite element results are now reasonable; however they are still not as accurate as those of the short TX-RX offset. Now that a mesh had been found that produced reasonable matches with the 1D analytic algorithm for long TX-RX offsets the resistive disk can be introduced.

3.2 Resistive Disk

3.2.1 Transmitter Frequency and Radius

The resistive disk is inserted into the double half-space with the following parameters; a range of frequencies (0.005 Hz to 1.0 Hz), seawater conductivity of 3.0 S/m, and a seafloor conductivity of 1.0 S/m. The newly introduced disk has a conductivity of 0.01 S/m. The first results are for a transmitter location of z = -100 m, and x = -1000 m with a variable radius of the disk (Fig. 8-11). This TX location is chosen in order for the receivers (0-20 km) to be at least one seawater skin depth (912 m) away from the transmitter when using the 0.1 Hz frequency. The seawater signals can be considered noise in this case and are unwanted. This noise attenuates rapidly and a much better subsurface signal to noise ratio is found at 1000 m from the transmitter location.

A study of the responses at varying transmitter frequencies is made to observe the offset between the double half-space and the infinite disk curves, as well as the behavior of the finite disks (1250 m, 2500 m, and 5000 m). When the disk is in the subsurface it is buried at 525 m. A suite of frequencies is run from 0.005 Hz to 1.0 Hz including 0.01 Hz, 0.02 Hz, 0.05 Hz, 0.1 Hz, 0.2 Hz, 0.5 Hz, and 0.8 Hz. The skin depths of these frequencies in both seawater and seafloor sediments can be found in Table 2.

The results show that for the group of lowest frequencies the curve separation is not significantly decisive (Fig. 8). The lower frequencies show the greatest offset between the double half-space curve and the infinite disk curve. However, the offset occurs during the short range set of the receivers, from 625 m to about 4000 m. This occurs for the three lowest frequencies: 0.005 Hz, 0.01 Hz, and 0.02 Hz. These low frequencies show little to no curve separation at distances greater than 4000 m. This is likely due to the receivers at these locations collecting signals from currents which have preferentially been induced in the host medium beneath the disk. The next group of frequencies better visualizes the disk.

The middle frequencies of 0.05 Hz, 0.1 Hz, and 0.2 Hz (Fig. 9) show a small amount of curve separation at all receiver positions from 625 m to over 10 km. The offset is mostly consistent along the x-axis receivers with little variation. These frequencies appear to be probing the disk more consistently than the previous frequencies because the curves of the double half-space results and the infinite disk results do not overlap. A trend can also be noticed in the finite disks, where they grade from the infinite disk behavior at short TX-RX offsets to double half-space behavior at long TX-RX offset. As the frequency increases the gradation of the finite disks occurs at shorter

TX-RX offsets. This is seen by comparing long TX-RX offset finite curves for the middle frequencies and high frequencies (Fig.11).

The highest frequencies include 0.5 Hz, 0.8 Hz, and 1.0 Hz (Fig. 10). The results are similar to the previous group in that they show a consistent offset between the two end-member curves along the receiver profile. Significant electromagnetic energy appears to be propagating through the disk and not entirely under or above the disk. The curve separation is slightly decreased from that of the previous group which may indicate that not as much energy is getting through the disk. The pattern is tending towards an overlap of the results of double half-space curve and the infinite disk curve. This may be due to the decrease in depth of penetration as the higher frequencies are considered. The finite disk response curves continue to show a decrease in the TX-RX offset at which the curves follow the behavior of the double half-space. The depths to the disk are about one skin depth (for these high frequencies) which means that less energy than in the case of the middle frequencies propagates through the region of sediments containing the disk. It is hypothesized that even higher frequencies would result in a complete overlap in the double half-space scenario and the infinite disk scenario as the frequencies would not be probing to the depth of the disk. However, at this time higher frequency scenarios cannot be run as the finite element calculations become unstable. The ideal frequency for the model we have been running is ~0.1 Hz (Fig. 12). This frequency provides the best separation between the double half-space and infinite disk curves.

The finite disk responses are important in that they test the cylindrical 3D capability of the FE algorithm. The responses show a gradation from infinite disk behavior at short TX-RX offset and double half-space (no disk) behavior at long TX-RX

offsets. This gradation occurs at receivers which are located on the x-axis past the edge of the buried disk. The lag occurs as the signals containing information about the edge of the disk do not travel to the receivers directly above the disk, but to receivers further down the x-axis. Therefore the edge of the finite disks can be roughly located with these techniques.

The conclusions that can be made from this section are simple, yet very important for experimental design. The frequency should be carefully chosen based on the depth of the structure that is trying to be observed. A high frequency that yields an excessive attenuation does not penetrate to the depth of the object. Low frequencies probe much deeper and may only be observing the subsurface below the desired target. The other important conclusion is that finite disks begin to behave similar to the double half-space rather than the infinite disk at shorter TX-RX offsets as the frequency increases. This model may be a useful in deciding which frequency to use in experiments.

3.2.2 Disk Depth

The disk is buried at three different depths (Fig. 13). The original burial depth used had been 525 m. The disk is raised to 225 m and lowered to 1012.5 m. These depths are chosen somewhat arbitrarily mainly to observe the change in behavior of the total electromagnetic fields. The two changes that are observed in Fig. 13 are the strength of the total electric field and the separation between the different responses of the different disk radii.

Each disk depth shows a significant difference in the behavior of its total electric field response. The shallowest burial depth of 225 m below the seafloor shows little

separation between the double half-space scenario and the infinite disk scenario as signals are probing mainly the sediments beneath the disk. The responses from the finite disks grade from the infinite disk response to that of the double half-space response at large TX-RX offset. The largest disk, 5000 m, as expected changes over at the greatest TX-RX offset.

The next disk depth is the standard depth used in the other scenarios which is 525 m. The separation of the double half-space and infinite scenario curves has increased at large offset, while decreasing slightly at short offset from the 225 m burial depth case. The decrease could be due to the receivers sampling only shallow penetrating electromagnetic fields which do not penetrate deep enough to sense the disk. The opposite is true in the cases of large TX-RX offset as these receivers contain a significant amount of data probing the depth ranges containing the disk. As in the case of the 225 m burial, the finite disk responses grade from the infinite disk case to the double half-space curve, but do so at slightly larger TX-RX offsets. This again is due to the fact that the disk is buried deeper, so the seafloor signals from fields diffusing through the disk are not read by the closer receivers. The slight lag between the location of the edge of the disk and the location of receivers which apparently contain that information (in the form of the beginning of the crossover from infinite-disk and no-disk) are seen once again.

The last depth chosen and the deepest is 1012.5 m. The offset in this case between the double half-space and infinite disk scenarios is slightly increased from that of the 525 m burial. Once again the short TX-RX offset data shows a decrease in separation due to the deep burial of the disk. The finite disk curves behave in a predictable manner in that they grade from the infinite disk curve to the double half-space

curve, but due so at receivers slightly further from zero than in the 525 m case. This is also due to the increased depth of burial.

The depth of burial of the resistive body has a significant impact on the differences between responses for models with various disk radii. The ability to distinguish the curves increases significantly from a burial of 225 m to 525 m, but not from 525 m to 1012.5 m. This is suggesting that another factor is controlling the curve separation with depth. This factor may possible be related to the frequency of the transmitter, since changing frequency effectively changes the depth of penetration.

3.2.3 Transmitter Location

The transmitter is then moved away from zero along the x-axis in steps of 1000 m. The receiver results from offsets ranging from 0 to 20 km are predictable in that they decrease in strength as the transmitter moves outward (Fig. 14). The TX location of XTX = -1000 m is an exception in that it produces weaker responses than the next TX position further away from zero (XTX = -2000 m). One reason for this may be that the receivers close to the TX contain an increased amount of information from fields diffusing through the seawater. The fields traveling through the seawater attenuate over shorter distances and may be producing the weakened results at XTX = -1000 m.

The large TX-RX response of the infinite disk scenario for XTX = -1000 m produces results varied from other TX locations. One explanation for the unusually strong infinite disk response may be that the EM fields become trapped in the resistive layer and diffuse along its length. This may be analogous to the wave guide phenomena

in seismic methods. The EM fields attenuate much less as they travel through the low conductivity layer which results in anomalously strong responses at great distances.

The more distant transmitter locations exhibit weaker receiver signals, but provide greater distinction between the various disk responses. At transmitter locations of -3000 m to -5000 m the curves for the double half-space and infinite disk scenarios are separated at short TX-RX offset which was not the case for transmitter locations nearer to zero. These scenarios show that information can be gained from certain locations which more clearly display the subsurface geometry.

3.3 Disk Thickness

Now that the one layered disk has been studied the next step is to increase the disk thickness to observe the effects on the total electric fields. The top of this 3-layered disk is again at 525 m depth beneath the seafloor. The models include the extremes of no-disk and infinite-disk as well as the three finite disks (1250 m, 2500 m, and 5000 m). The same range of transmitter frequencies, 0.005 Hz to 1.0 Hz is used. The transmitter is located at -1000 m on the x-axis.

The results (Fig. 15-17) are very similar to those of a 1-layered disk. The lowest three frequencies of 0.005 Hz, 0.01 Hz, and 0.02 Hz (Fig. 15) show a large separation between the double half-space curve and the infinite disk curve at short offset. As in the case of a one-layered disk, the long offset receivers show little separation in the readings for the total electric fields. This is most likely due to the low frequency electromagnetic fields preferentially propagating underneath the disk and probing the properties of the sediments below. The main difference between these results and those of the 1-layered

disk is that the disk curves show a total electric field which is slightly stronger in the 3-layered disk scenario. This is due to the thicker structure and results in a greater separation from the double half-space scenario.

The 3-layered disk responses at the middle frequencies (Fig. 16) show very similar properties to those of the 1-layered disk. They show constant curve separation from receivers at 625 m to over 10 km. This again shows that the total fields contain information about the disk at short and long TX-RX offset, unlike the low frequency results. Once again the disk curves show slightly stronger total electric fields due to the thickened disk, which results in a larger separation than in the 1-layer disk scenario. The finite disks behave in a similar manner as the models with the single-layered disk. However the crossover in behavior occurs at larger TX-RX offsets due to the increased disk thicknesses.

The responses of the three highest frequencies (Fig. 17) are predictable. The separation between the double half-space and infinite disk curves has decreased from that of the lower frequencies due to a decrease in the depth of penetration so that induced currents flow largely above the disk. The disk curves also show slightly increased strengths in the total electric field from responses in the 1-layered disk scenario. Once again the finite disks show crossover at greater TX-RX offsets than the single-layered models (Fig. 18).

The thickened disk results reveal important information despite the slight changes. An easily predictable result is that the strength of the total electric field increases as the thickness of the structure increases. The finite disks crossover from the response of an infinite disk to that of the double half-space at larger TX-RX offsets as the

thickness of the disk increases. The relative separation between the double half-space and infinite disk curves remain about the same for each of the different transmitter frequencies, as in the single-layered disk. Therefore the same frequency that is best for the 1-layered disk is probably also best for the 3-layered disk. This may not be true for drastically increased thicknesses which have not been examined here. Now that the thickness parameter has been altered and its effects understood the geometrically complex structure will be studied.

3.4 Complex Structure

Evaluating the EM response of the structure which represents a rough design of a hydrocarbon reservoir is the final step in this research. The description of the structure is found in the experimental design section 2.4 and drawn in Fig. 3. The first objective is to determine which frequency is best at locating this specific structure. The second and last objective is to determine if locating the shallowest portion of the reservoir, and hence the most productive part, is feasible.

3.4.1 Transmitter Frequencies

The range of frequencies is the same as used in the 3-layered disk. The first results (Fig. 19) are for all 9 frequencies running from 0.005 to 1.0 Hz at a burial depth of 525 m and with the structure facing towards the negative side of the x-axis. The TX location is at XTX = -1000 m and the structure is ~112 m thick. The results are very similar to those of the 1-layered disk and the 3-layered disk. The lowest frequencies of 0.005 Hz, 0.01 Hz, and 0.02 Hz show a large difference between the double half-space

curve and the structure curve at short TX-RX offset. Once again this seems to indicate that these frequencies, being the lowest, are propagating preferentially underneath the structure which is buried at the same depth as the previous structures. This makes the same sense as before and also suggests that the FE code generates consistent results.

The middle frequencies, consisting of 0.05 Hz, 0.1 Hz, and 0.2 Hz, show results consistent with previous structures. The offset at small range has decreased from the lowest frequencies, but the long range receivers are beginning to show a difference between the double half-space response and that of the structure. An important note is that the structure is finite yet is still being observed by the receivers over 10 km (several skin depths) distant. The infinite curves of the single and three-layered disk show an offset from the double half-space larger than that of the structure. This predictable fact ensures that the FE code is working in accordance with expectations.

The three highest frequencies also begin to show a predictable decrease in offset between the double half-space response and the structure response from that of the middle three frequencies. The short range receivers show a separation between the two curves which shows a slight decrease as the frequency increases. The long range receivers show a convergence of the two curves indicating that the long range receivers are not imaging the structure. This could be the result of the finite nature of the structure. Looking back at the frequency range plots of the single and triple-layered disks it is seen that even the highest frequencies still image their respective buried structures. This is due to the fact that the disk plots include results of infinite radii. This seems to be indicating further evidence that the solver is properly modeling the natural world as the finite structure is producing weaker signals at long range than the infinite disks.

A parameter that is being tested simultaneously with the transmitter frequency is the effect of the structures orientation. The code would be viewing the 3D nature of the structure if the responses from the three different orientations facing the negative x-axis, positive x-axis and positive y-axis displayed differences. The reason that the latter two plots are not shown is because they exhibit the same responses as Figure 18 where the structure is facing the negative side of the x-axis. The 3D nature of the structure is not being imaged. The burial depth is then decreased to attempt to display differences in the three orientations.

The next set of models in the frequency experiment included the same range of frequencies and three orientations, but the burial depth is now 225 m. The responses (Fig. 20) are very much the same in terms of the curve patterns. The one difference which would be expected is that the 225 m burial produced stronger responses from the structure model. This in turn caused a greater offset between the structure response curves and the double half-space curves. The reason for the stronger structure responses could be attributed to the structure being probed by higher powered signals as they have traveled even less of a skin depth than those signals probing the deeper (525 m) structure. The three different orientations once again produced the same exact responses for a burial depth of 225 m; indicating that the 3D nature of the structure is not being imaged..

The main purpose of this frequency range experiment is to decide which frequency was ideal for looking at this structure and to show the 3D nature of the structure. The frequency that is chosen in this case was 0.1 Hz. This is the same frequency that was chosen for the single and triple-layered disk. The reason that this frequency is chosen is because it exhibited the most consistent offset over the range of

receivers from about 600 m to over 10 km. This frequency will now be used in the second determination for locating the shallowest part of the structure. The 3D nature of the structure is not displayed in the responses as all three orientations at both burial depths of 225 m and 525 m produced the exact same curves.

3.4.2 Structure Depth

The structure is buried at the same three depths as that of the single-layered disk (225 m, 525 m, and 1012.5 m). The responses (Fig. 21) are similar to those of the single-layered disk. At a burial depth of 225 m the structure is imaged well at short to middle ranges, but at ranges approaching 5000 m the structure responses are weaker as the receivers at these distances contain more information about the sediment below the structure than the structure itself. The opposite is true for the second two burial depths. A burial depth of 525 m produces the strongest offsets of double half-space responses and structure responses past about 1000 m on the x-axis. The receivers located before 1000 m are reading signals more dominated by the sediments above the structure then the receivers located after 1000 m. This pattern is exhibited even more so in the 1012.5 m burial depth. The receivers located 2000 m from zero and beyond show the strongest differences between the double half-space curves and the structure curves.

This information contained in Fig. 21 is important in much the same way as that of the single-layered disk depth results (Fig. 13). The burial depth of the desired object is an important piece of information to know when choosing the most appropriate frequency.

3.4.3 Structure Orientation

The second objective to locate the shallowest point of the structure is done by looking at the structure from different perspectives and by using various transmitter locations. The three different orientations are with the structure open face directed towards the negative side of the x-axis, the positive side of the x-axis and the positive side of the y-axis. The structure is observed from six transmitter locations moving away from XTX = 0 m and from two burial depths (225 m and 525 m). The TX frequency used is 0.1 Hz and the thickness of the structure is ~112 m. The strengths of the signals decrease as the transmitter is moved away from the structure. The double half-space curves and the structure curves show a separation which decreases as transmitter position moves further from the center of the mesh. Now that the general characteristics of these curves have been covered, the difference between the orientations will follow.

The three different orientations listed above are chosen to look at the structure from different sides to look for slight variations which may indicate certain aspects of the structure's geometry. The responses for the three orientations are identical for the burial depth of 525 m (Fig. 22). The same is true for the burial depth of 225 m (Fig. 23). This indicates that the signal is not changing despite changes in the geometry of the subsurface. This is not to say that any structure would not result in a signal change, only perhaps structures of this scale. The fact that there is no difference in these six plots seems to indicate that the small changes in the geometry of the structure cannot be seen with this particular experimental design. This further indicates that locating the shallowest portion of the structure where a well might be located cannot be found with

this design. The next and last parameter to alter in this study is the thickness of the structure.

3.4.4 Structure Thickness

The structure is thickened from its original (~112 m) to ~336 m and ~675 m. The depth of burial remains at 525 m and the frequency stays at 0.1 Hz. The transmitter locations move out from 0 m to -5000 m on the x-axis in steps of 1000 m.

The first increase in thickness from ~112 m to ~336 m shows no significant difference in the responses (Fig. 24). The thickness increase does cause the total field strength to increase as the amount of travel distance through the structure has increased relative to the distance traveled through the sediments. Despite tripling the thickness the three different orientations show no difference in their responses indicating that the geometric changes in the structure are still not observed in the responses.

The last thickness increase is from ~336 m to ~ 675 m and exhibits responses (Fig. 25, 26) which show that the structure is not radially symmetrical. The offset between the structure curves and the double half-space curves again increased due to the thickness of the structure increasing. An additional plot (Fig. 27) has been created to better exhibit the differences between the two orientations. The plot compares the response curves from the structure's open side facing the negative side of the x-axis and facing the positive side of the x-axis. The differences between the two orientations responses can be seen in the receivers at short offset from the zero location at TX locations of -3000 m, -4000 m, and -5000 m.

When the structure is facing the negative side of the x-axis it produces a stronger response than when it is facing the positive side of the x-axis (Fig. 28). Since the receivers are on the positive side of the x-axis this response is predictable as the signals are traveling through a greater portion of the structure when it is facing open towards the negative side of the x-axis. When the structure is open towards the positive side of the axis more of the sediments are being probed, the main difference being the sediments in the open segment of the structure. These responses do not seem to directly indicate where the shallowest portion of the structure is located. However it has been shown that the 3D nature of this structure can be seen in the response curves.

The conclusion of these trials is that the shallowest portion of the resistive body cannot be imaged with these parameters, but the 3D nature of structures can be observed. The 3D nature of the structure may not be well defined from these experiments, but they have been observed. It may be that higher frequencies may better display the 3D structure.

4. CONCLUSIONS AND DISCUSSION

The use of a finite-element 3D forward modeling algorithm can be useful to obtain information that will increase understanding of controlled-source EM responses. It was shown that various size finite disks will behave as an infinite disk at short range while grading into the behavior of a homogeneous double half-space at larger TX-RX receiver offset. The larger the radius of the disk means that crossover occurs further from the transmitter. Changing the disk depth from 225 m to 525 m resulted in significant changes in the responses indicating that disk depth played an important role. However the lack of significant change from 525 m to 1012.5 m indicated that there was another parameter with significant effect involving the transmitter.

The two parameters that were shown to have a significant impact on the total electric field were the transmitter location and the transmitted frequency. When multiple transmitter positions were modeled the results showed a decrease in signal strength as the transmitter moved further away, but showed greater separation between the infinite disk and double half-space curves. Thus multiple transmitter locations can provide different useful information. The transmitted frequency is important in that it determines the depth to which the field will penetrate. A frequency of 0.1 Hz was chosen for these experiments because it showed a constant separation in the double half-space curves and the infinite disk curves, as TX-RX offset was varied, indicating that this frequency imaged the disk well in the models that were run. Changes in the design of the subsurface feature played an important part of the understanding of CSEM methods as well.

The results for the geometrically complex structure showed that changes on the scale of 100s of m could be seen in this experimental design. The first step in tripling the thickness of the disk gave important information in that it confirmed an increase in signal strength due to an increase in structure size. Although the lack of change in the complex structure results at thicknesses of ~112 m and ~375 m, valued information was gained. Once the structure was thickened six times the original it was learned that the 3D geometric changes in structure is better resolved with these designs. However the model suggests that the differences were small. It is hypothesized that higher frequencies and additional electrical information (E_y) may better image the structure. These experiments have been shown to result in useful information for real world experimental design with CSEM as well as show the usefulness of this finite element 3D forward-modeling algorithm.

The results for the experiments run may be simple, but are intuitive in terms of EM methods, and validate the accuracy and precision of this 3D forward modeling code. The code has shown results which validate the ideas of how EM works in a marine environment, but at the same time reveals the limits in terms of knowledge of CSEM methods. The problem of understanding the responses of CSEM methods is complex, but through the use of this code it has been shown that CSEM can be used to locate certain structures in the marine environment which may prove useful to the petroleum industry. The numerical algorithm is extremely complex at best, but flexible and useful. Future studies may be done with this code to create more stable results by determining which mesh designs fit with which conductivities and transmitter frequencies. This study is

barely tapping a huge reservoir of information that can be gained in the use of this 3D forward modeling algorithm.

REFERENCES

Badea, E.A., Everett, M.E., Newman, G.A., & Biro, O., 2001. Finite-element analysis of controlled-source electromagnetic induction using Coulomb-gauged potentials, *Geophysics*, **66**, 786-799.

Biro, O., & Preis, K., 1989. On the use of the magnetic vector potential in the finite element analysis of the three-dimensional eddy-currents, *IEEE Trans. Magn.*, **25**, 3145-3159.

Cairns, G.W., Evans, R.L., & Edwards, R.N., 1996. A time domain electromagnetic survey of the TAG hydrothermal mound, *Geophysical Research Letters*, **23**, 3455-3458.

Cheesman, S.J., Edwards, R.N., & Law, L.K., 1990. A test of a short-baseline sea-floor transient electromagnetic system, *Geophysics Journal International*, **103**, 431-437.

Cheesman, S.J., Law, L.K., & St. Louis, B., 1993. A porosity mapping survey in Hectate Strait using a seafloor electro-magnetic profiling system, *Marine Geology*, **110**, 245-256.

Constable, S., & Cox, C.S., 1996. Marine controlled-source electromagnetic sounding 2. The PEGASUS experiment, *Journal of Geophysical Research*, **101**, 5519-5530.

Constable, S.C., Orange, A.S., Hoversten, G.M., & Morrison, H.F, 1998. Marine magnetotellurics for petroleum exploration Part I: a sea-floor equipment system, *Geophysics*, **63**, 816-825.

Cox, C.S., Constable, S.C., Chave, A.D., & Webb, S.C., 1986. Controlled-source electromagnetic sounding of the oceanic lithosphere, *Nature*, **320**, 52-54.

Evans, R.L., Constable, S.C., Sinha, M.C., Cox, C.S., & Unsworth, M.J., 1991. Upper crustal resistivity structure of the East Pacific Rise near 13° N, *Geophysical Research Letters*, **18**, 1917-1920.

Evans, R.L., & Everett, M.E., 1994. Discrimination of hydrothermal mound structures using transient electromagnetic methods, *Geophysical Research Letters*, **21**, 501-504.

Evans, R.L., Sinha, M.C., Constable, S.C., & Unsworth, M.J, 1994. On the electrical nature of the axial melt zone at 13° N on the East Pacific Rise, *Journal of Geophysical Research*, **99**, 577-588.

Everett, M.E., & Edwards, R.N., 1992. Transient marine electromagnetics: the 2.5-D forward problem, *Geophysical Journal International*, **113**, 545-561.

Flosadóttir, Á.H., & Constable, S., 1996. Marine controlled-source electromagnetic sounding 1. Modeling and experimental design, *Journal of Geophysical Research*, **101**, 5507-5517.

Hoversten, G.M., Morrison, H.F., & Constable, S.C., 1998. Marine Magnetotellurics for petroleum exploration, Part II: Numerical analysis of subsalt resolution, *Geophysics*, **63**, 826-840.

Hoversten, G.M., Constable, S.C., & Morrison, H.F., 2000. Marine Magnetotellurics for base of salt mapping: Gulf of Mexico field test at the Gemini structure, *Geophysics*, **65**, 1476-1488.

MacGregor, L.M., Constable, S., & Sinha, M.C., 1998. The RAMESSES experiment—III. Controlled-source electromagnetic sounding of the Reykjanes Ridge at 57° 45′ N., *Geophysical Journal International*, **135**, 773-789.

MacGregor, L.M., Sinha, M., & Constable, S., 2001. Electrical resistivity structure of the Valu Fa Ridge, Lau Basin, from marine controlled-source electromagnetic sounding, *Geophysical Journal International*, **146**, 217-236.

Nobes, D.C., Law, L.K., & Edwards, R.N., 1992. Results of a sea-floor electromagnetic survey over a sedimented hydrothermal area on the Juan de Fuca Ridge, *Geophysical Journal International*, **110**, 333-346.

Sinha, M.C., Constable, S.C., Peirce, C., White, A., Heinson, G., MacGregor, L.M., & Navin, D.A., 1998. Magmatic processes at slow spreading ridges: implications of the RAMESSES experiment at 57° 45′ N on the Mid-Atlantic Ridge, *Geophysical Journal International*, **135**, 731-745.

Unsworth, M., 1994. Exploration of mid-ocean ridges with a frequency-domain electromagnetic system, *Geophysical Journal International*, **116**, 447-467.

Unsworth, M.J., Travis, B.J., & Chave, A.D., 1993. Electromagnetic induction by a finite electric dipole source over a 2-D earth, *Geophysics*, **58**, 198-214.

Young, P.D., & Cox, C.S., 1981. Electromagnetic active sounding near the East Pacific Rise, *Geophysical Research Letter*, **8**, 1043-1046.

Supplemental Sources

Badea, E.A., Everett, M.E., Shen, L.C., & Weis, C.J., 2001. Effect of background fields on three-dimensional finite element analysis of induction logging, *Radio Science*, **36**, 721-729.

Chave, A.D., & Cox, C.S., 1982. Controlled electromagnetic sources for measuring electrical conductivity beneath the oceans, *Journal of Geophysical Research*, **87**, 5327-5328.

Evans, R.L., Tarits, P., Chave, A.D., White, A., Heinson, G., Filloux, J.H., Toh, H., Seama, N., Utada, H., Booker, & J.R., Unsworth, M.J., 1999. Asymmetric electrical structure in the mantle beneath the East Pacific Rise at 17° S, *Science*, **286**, 752-756.

Everett, M.E., & Constable, S., 1999. Electric dipole fields over anisotropic seafloor: Theory & application to the structure of 40 Ma Pacific Ocean lithosphere, *Geophysical Journal International*, **136**, 41-56.

MacGregor, L.M., & Sinha, M., 2000. Use of marine controlled-source electromagnetic sounding for sub-basalt exploration, *Geophysical Prospecting*, **48**, 1091-1106.

Sinha, M.C., Patel, P.D., Unsworth, M.J., Owen, T.R.E., & MacCormack, M.R.G., 1990. An active source electromagnetic sounding system for marine use, *Marine Geophysical Researches*, **12**, 59-68.

Warren, S., 2004. Sea Change: Exxon Mobil bets on new technology in the hunt for oil, *Wall Street Journal*, Vol. **CCXLIV** No. 33 (August 17, 2004), p. A1, A6.

Webb, S.C., Constable, S.C., Cox, C.S., & Deaton, T.K, 1985. A seafloor electric field instrument, *Journal of Geomagnetism and Geoelectricity*, **37**, 1115-1129.

APPENDIX I: FIGURES

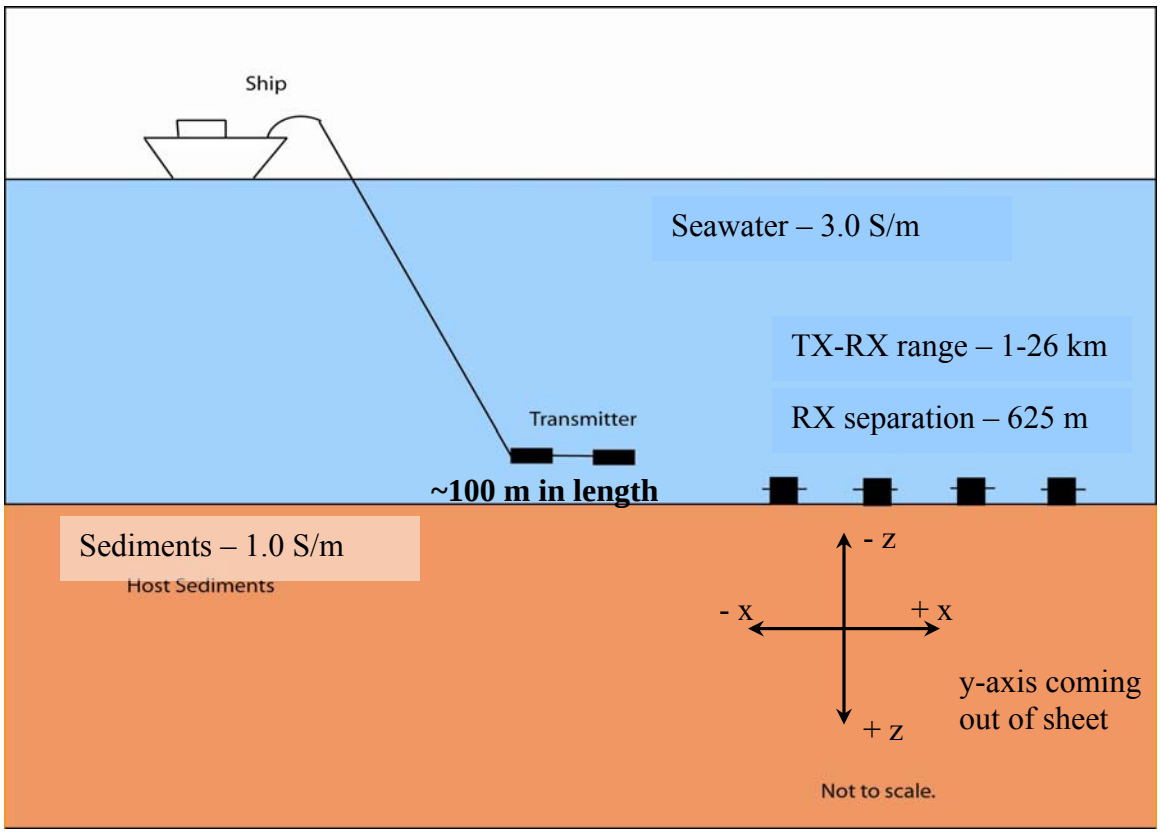

Figure 1 - A cartoon of an experimental setup over a double half-space.

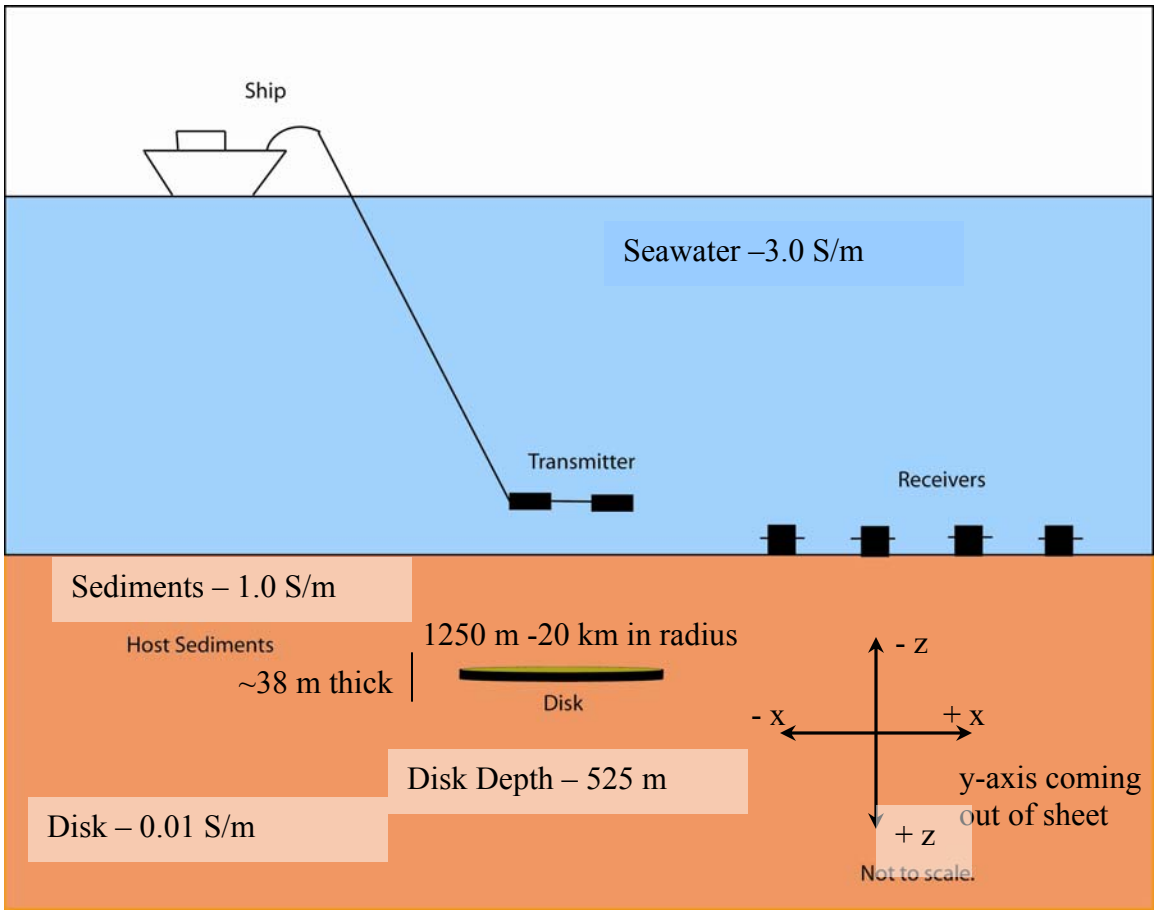

Figure 2 - A simplified drawing of the experimental setup over a disk.

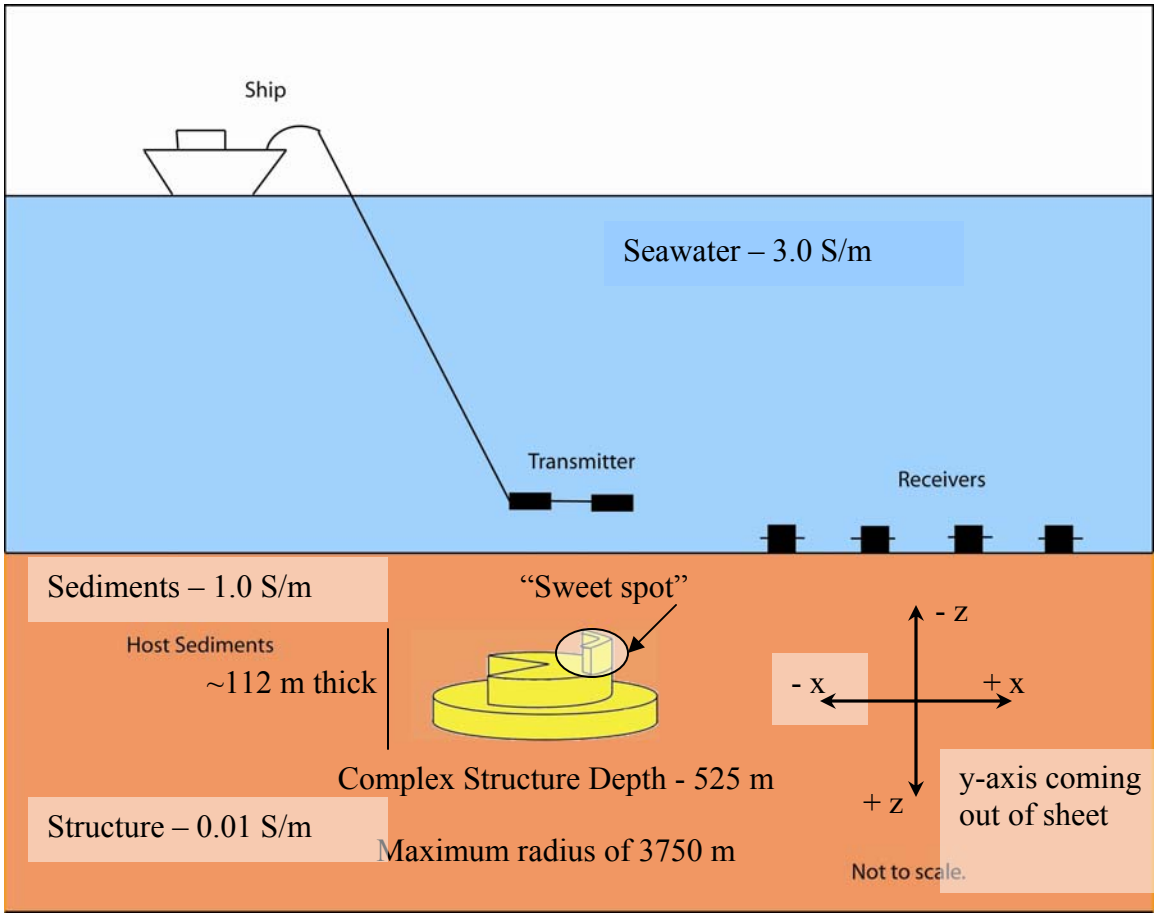

Figure 3 - A simplified drawing of the experimental setup over a complex structure.

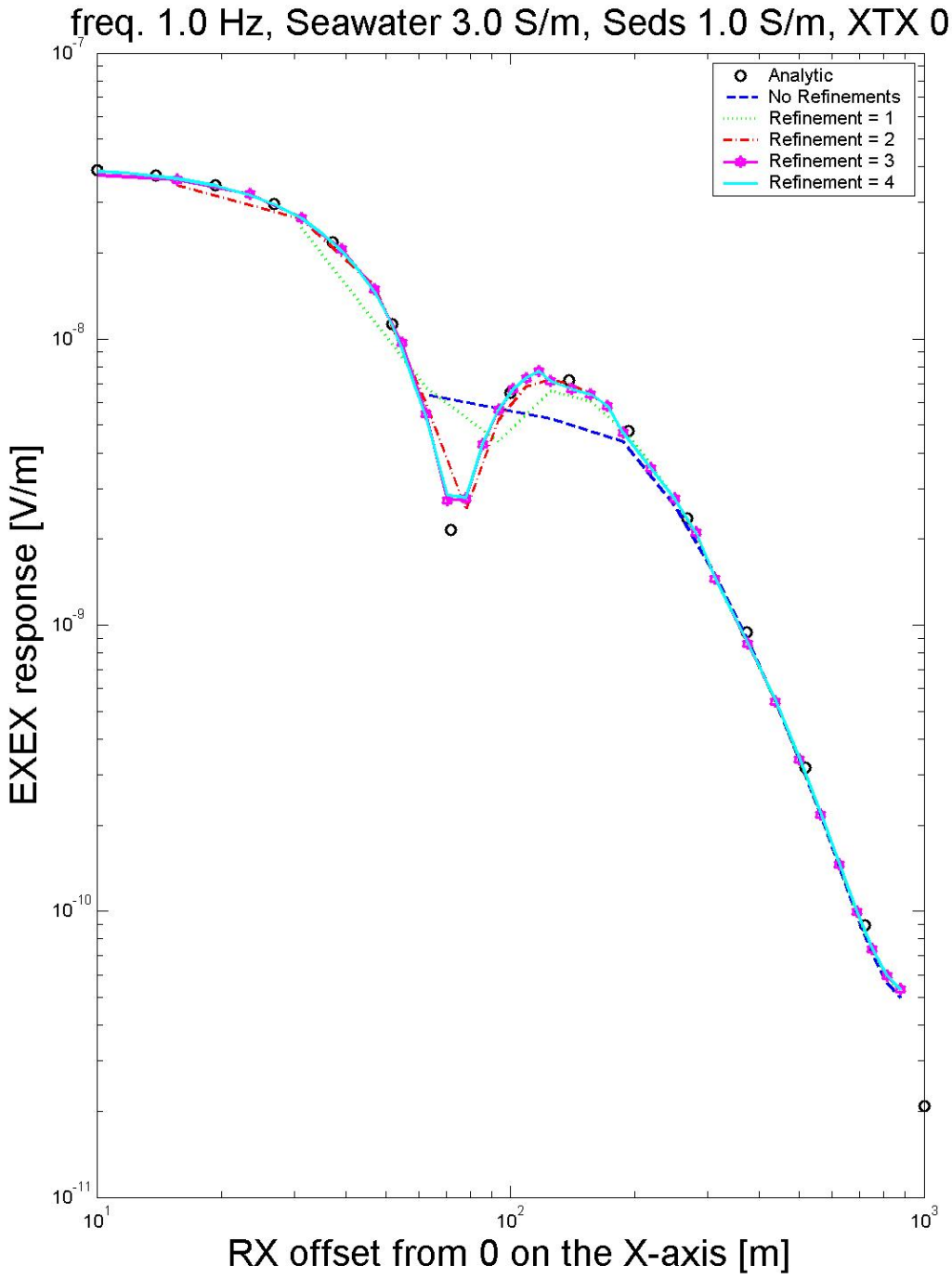

Figure 4 - A comparison of the 3D results with the 1D results for a double half-space.

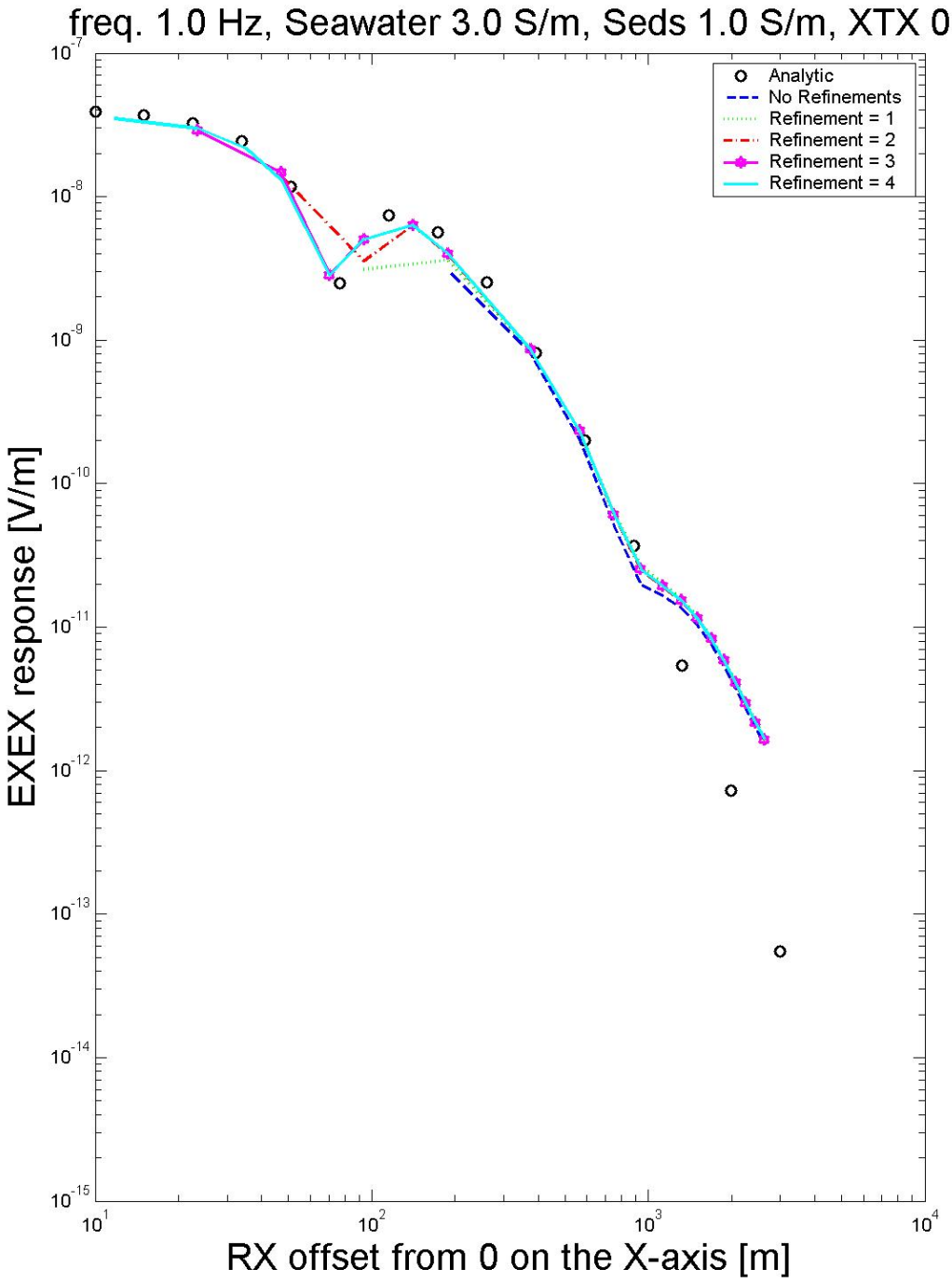

Figure 5 - A comparison of the analytic code results and the 3D FE offset for both short and long range receivers.

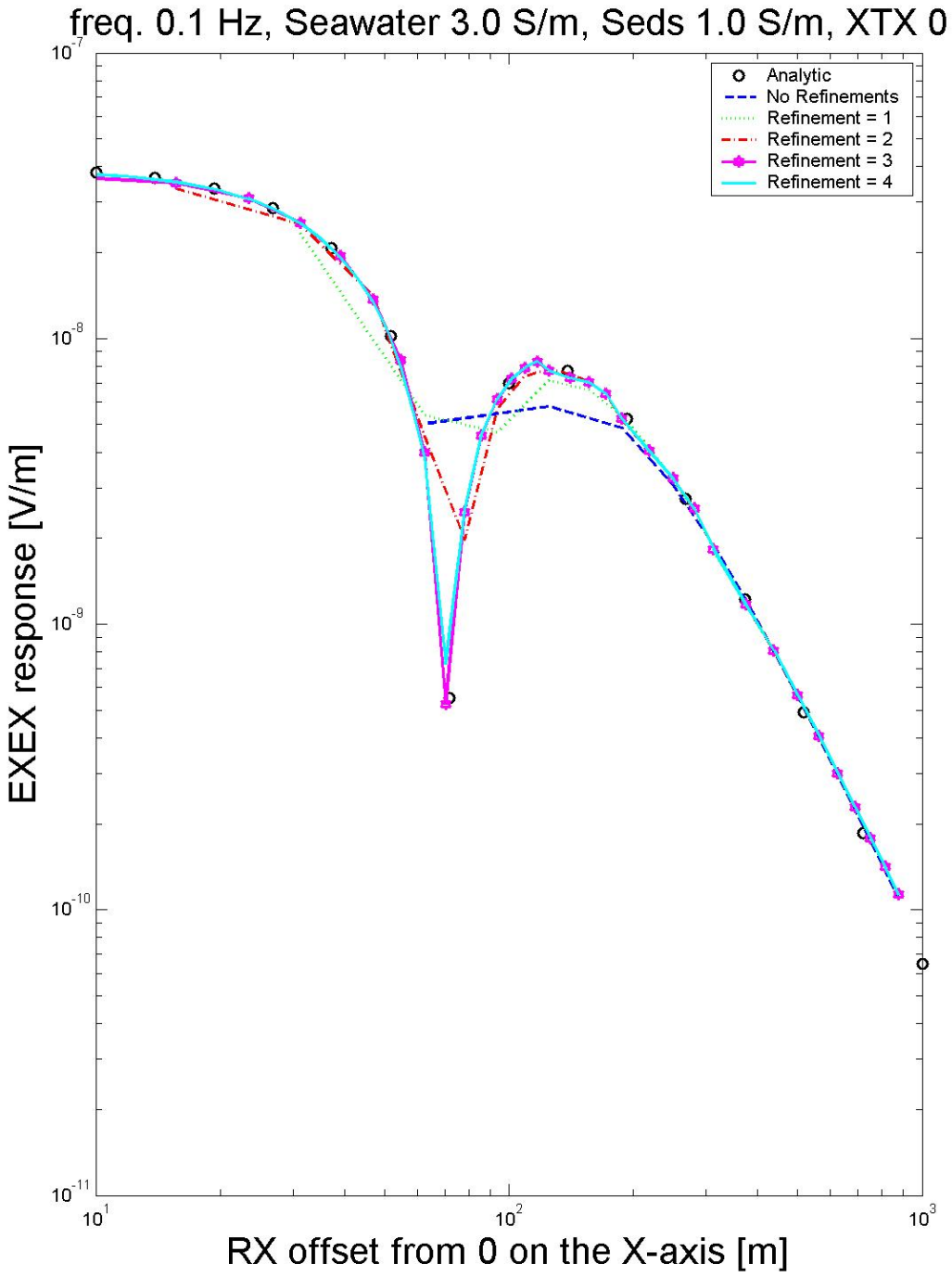

Figure 6 - A comparison of the 3D results with the 1D results for a double half-space.

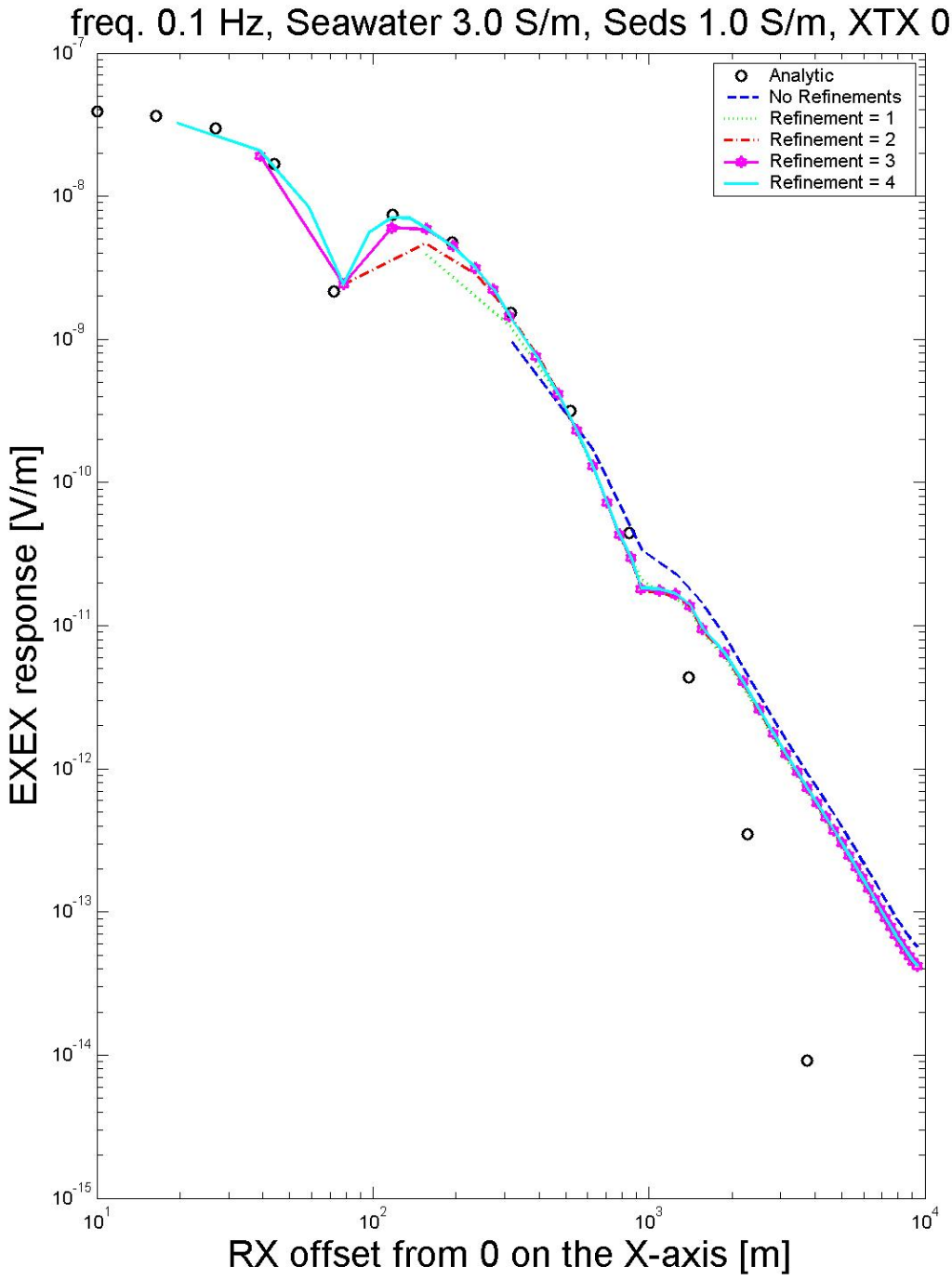

Figure 7 - A comparison of the analytic code and the 3D FE results for both short and long range receivers.

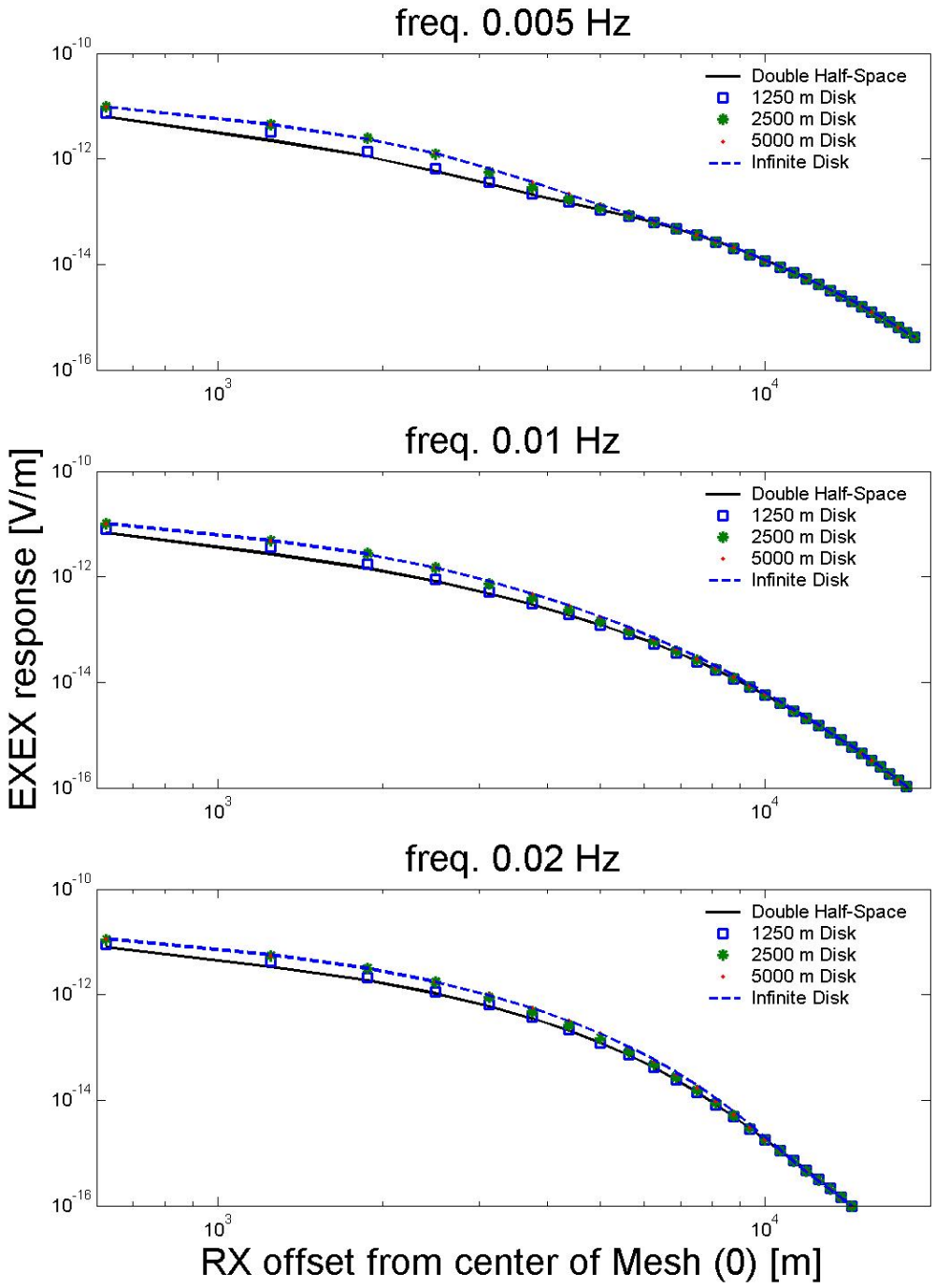

Figure 8 - The responses for the lowest transmitter frequencies. The transmitter is located at XTX = -1000 m and the single-layered disk is buried at a depth of 525 m.

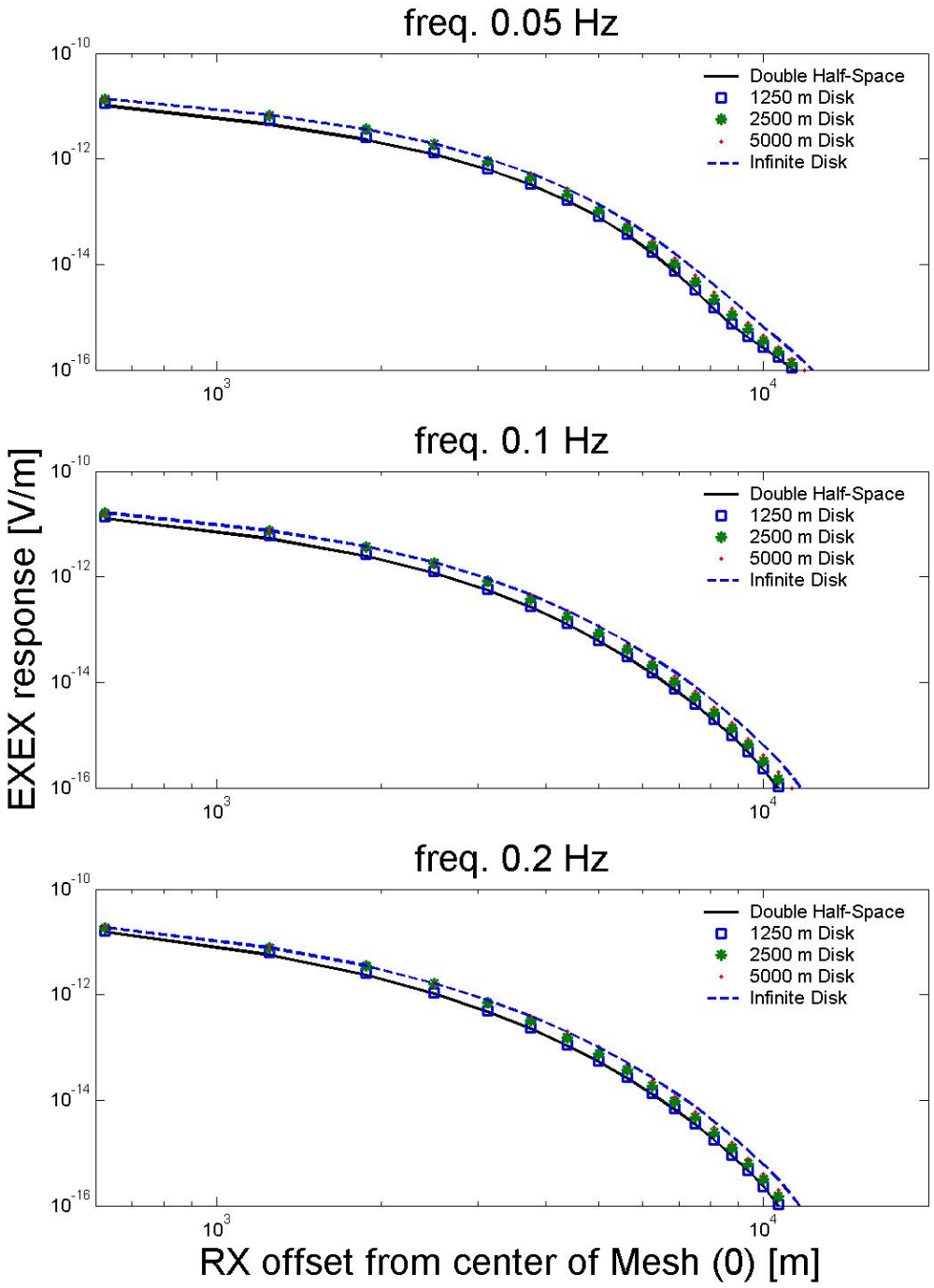

Figure 9 - The responses for the middle transmitter frequencies. The transmitter is located at XTX = -1000 m and the single-layered disk is buried at a depth of 525 m.

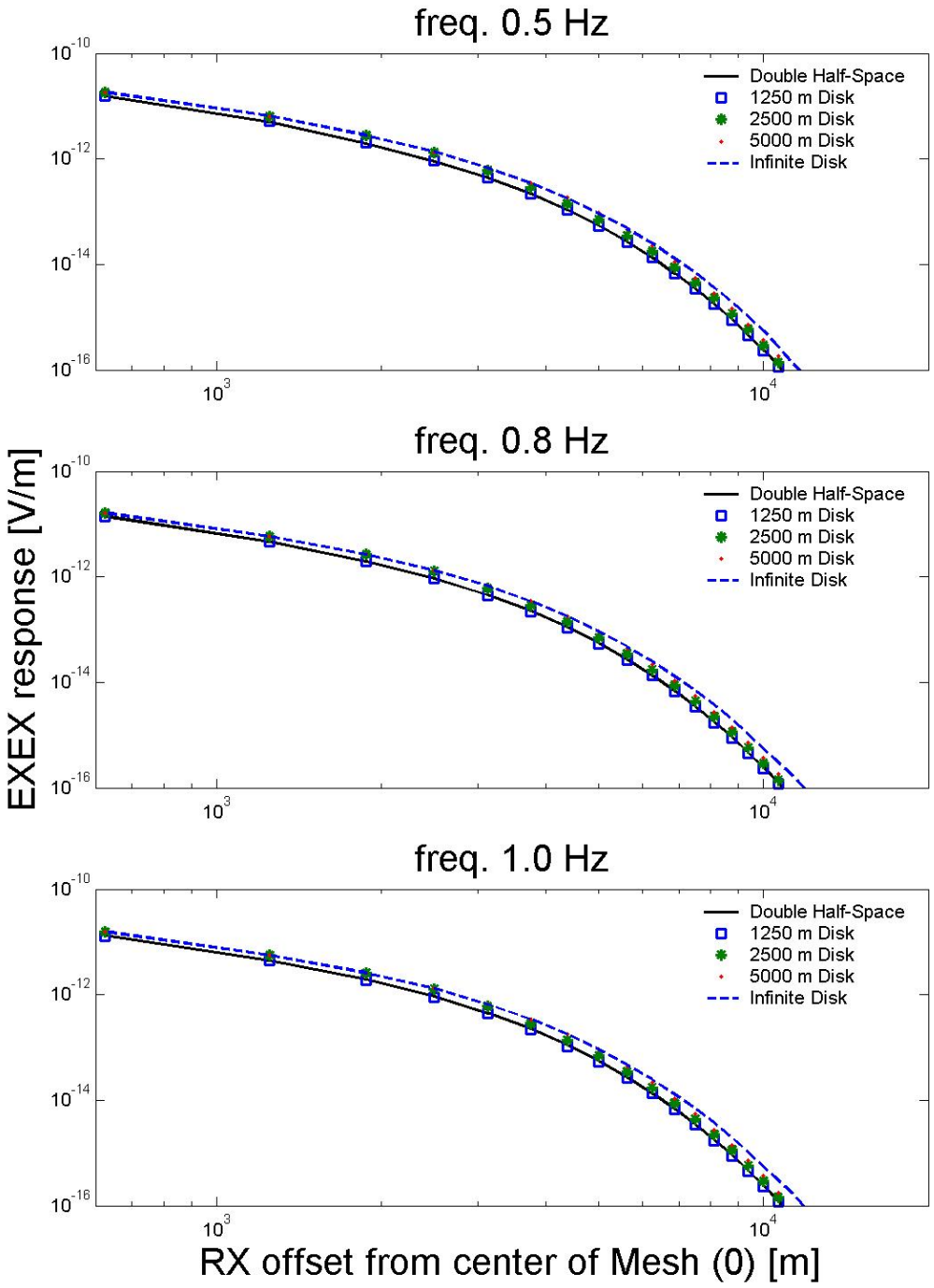

Figure 10 - The responses for the highest transmitter frequencies. The transmitter is located at XTX = -1000 m and the single-layered disk is buried at a depth of 525 m.

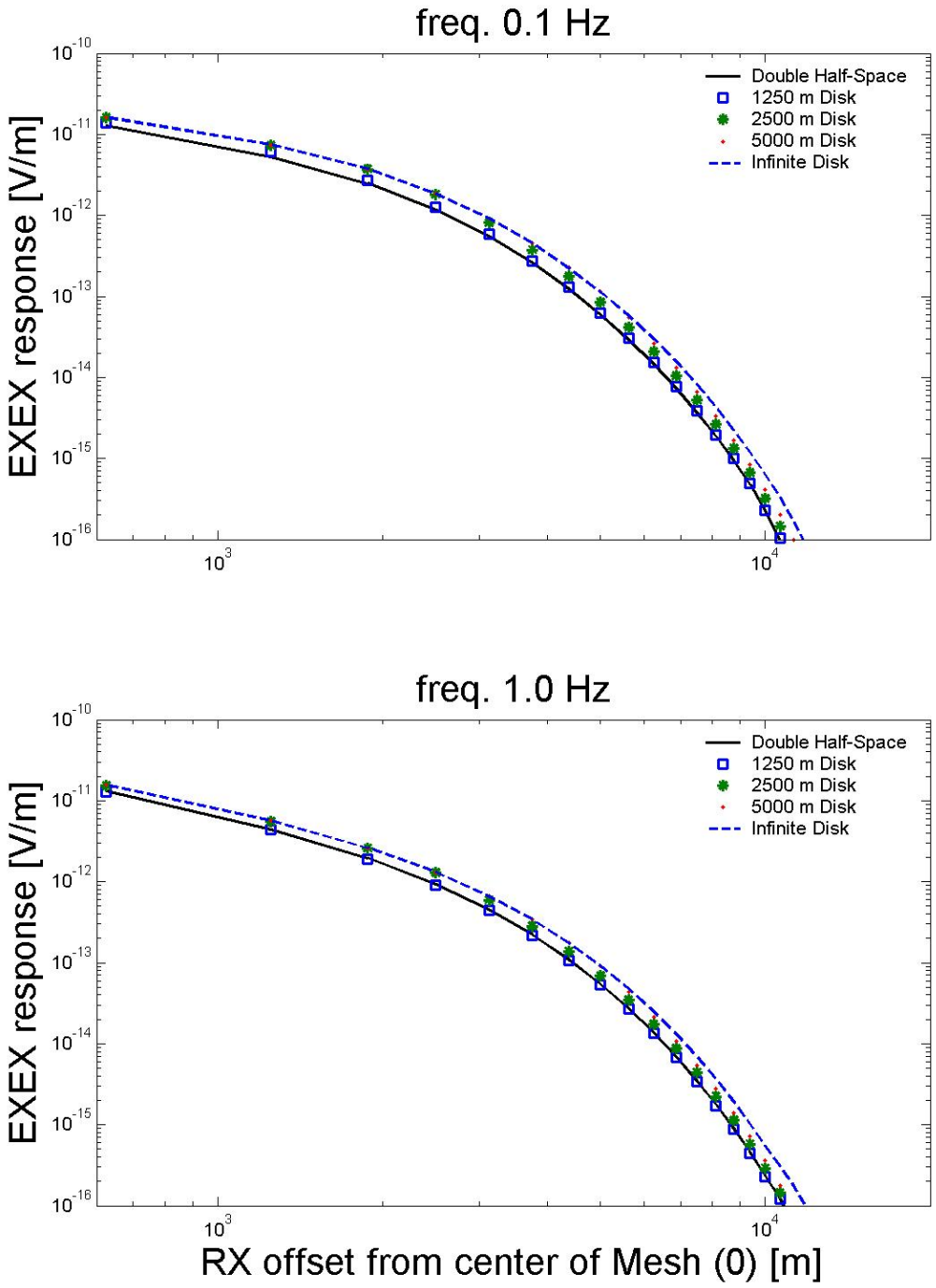

Figure 11 - Results from a model with a transmitter position of XTX = -1000 m, and a disk depth of 525 m.

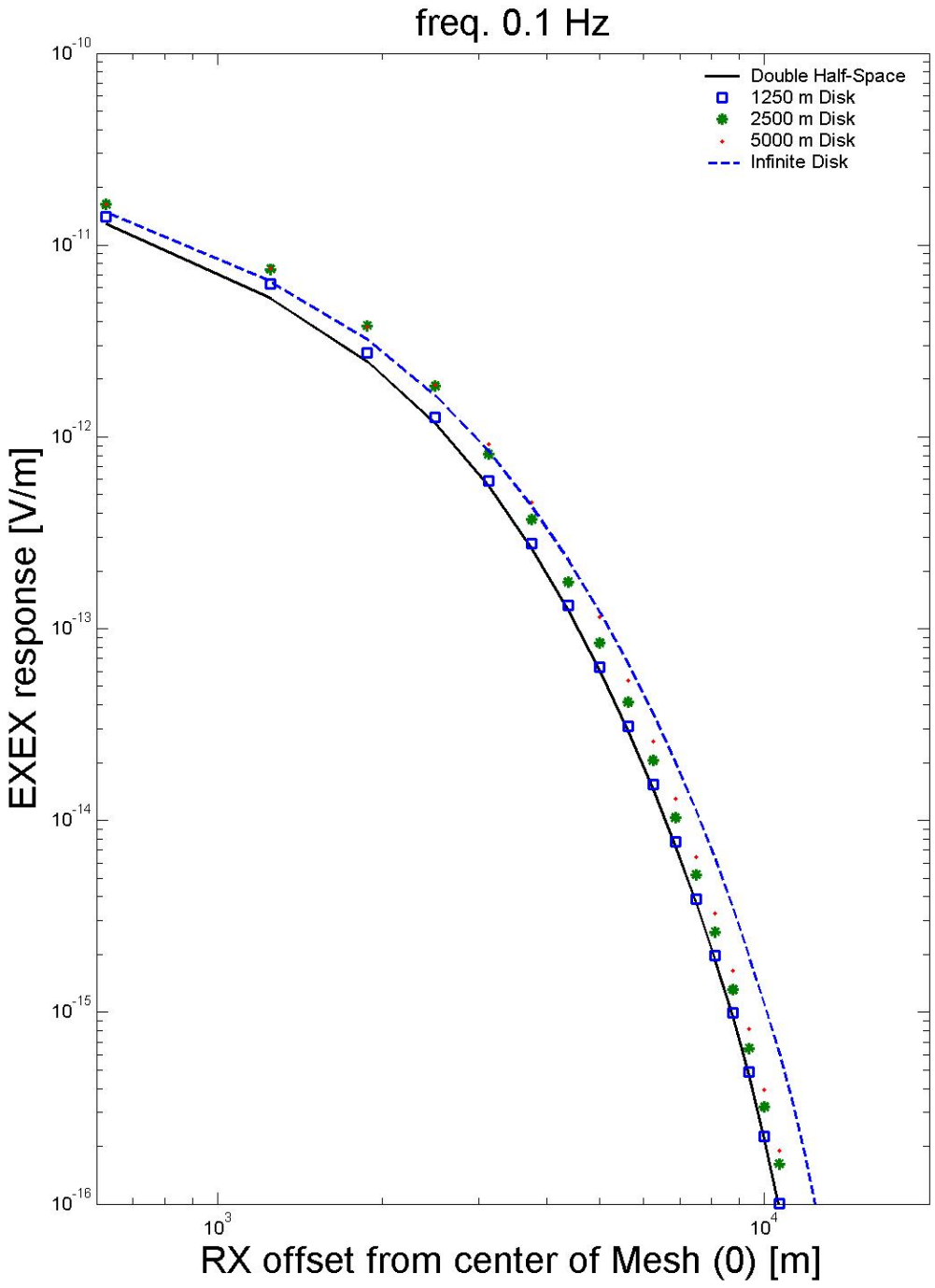

Figure 12 - Results from a model with a 0.1 Hz transmitter frequency, transmitter position of XTX = -1000 m, and a disk burial depth of 525 m.

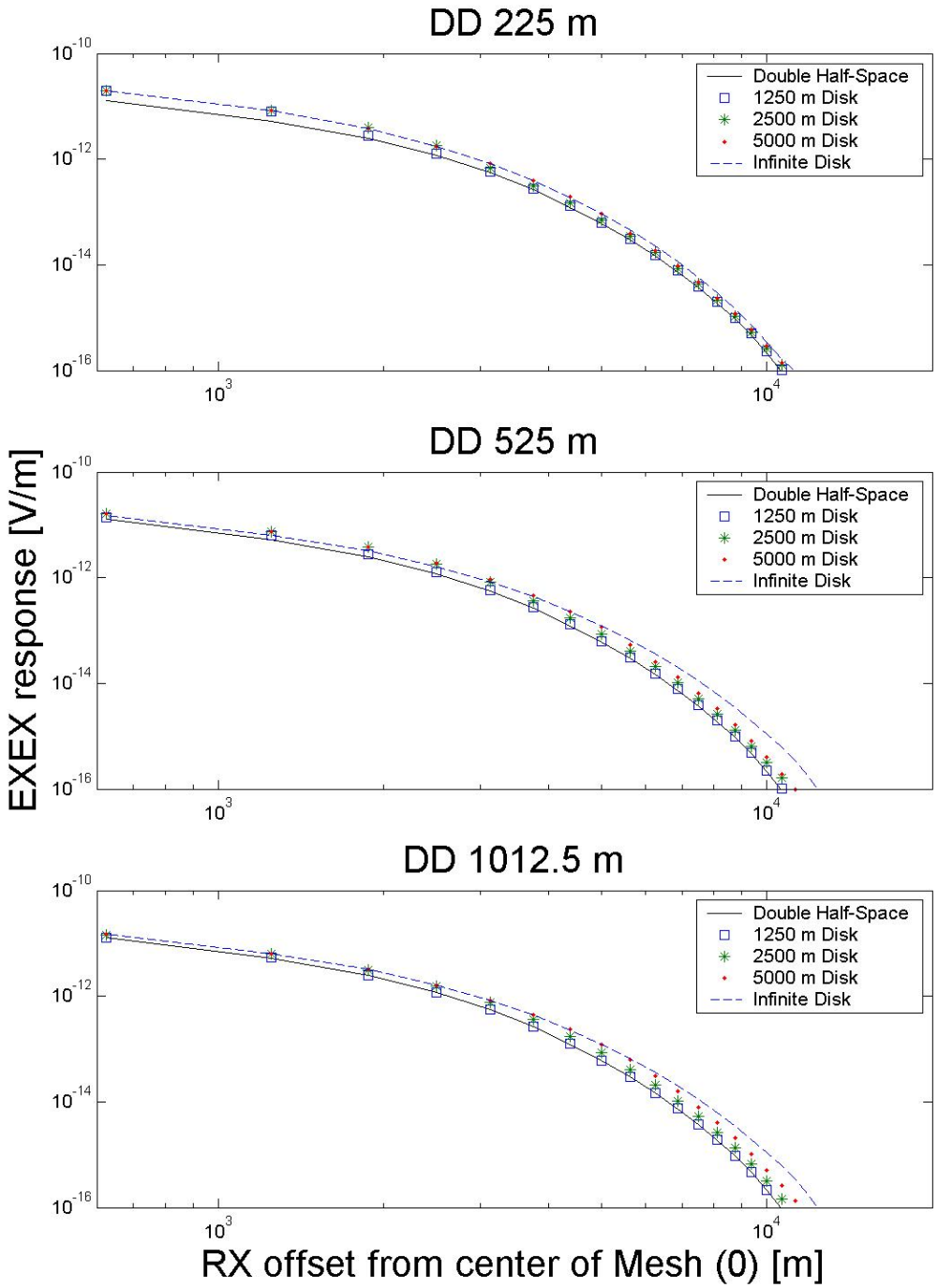

Figure 13 - Plots of responses for three disk burial depths. The transmitter frequency is 0.1 Hz and the transmitter location is at XTX = -1000.

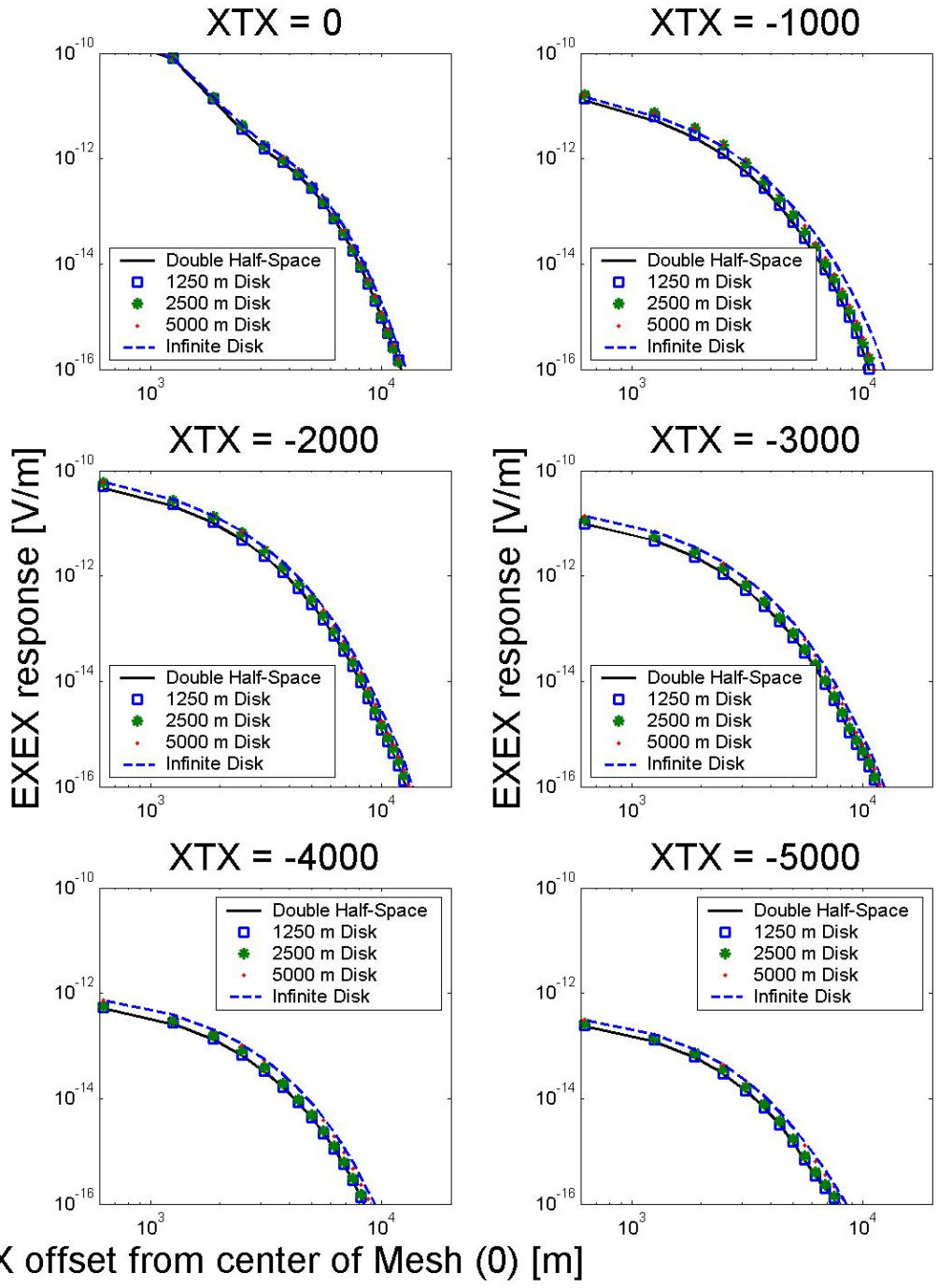

Figure 14 - Plots of various transmitter positions for a single-layered disk. The transmitter frequency is 0.1 Hz. The disk burial depth is 525 m.

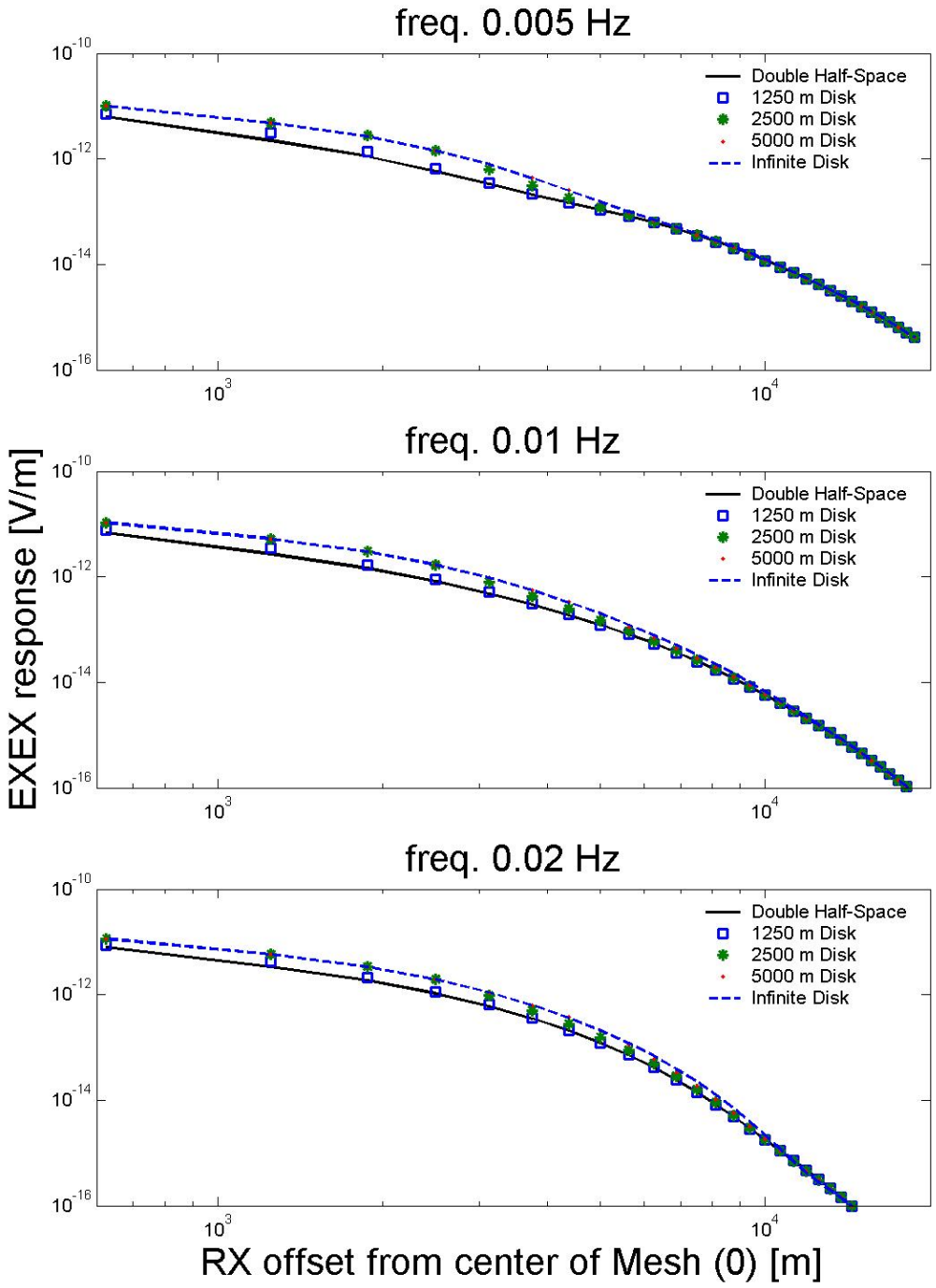

Figure 15 - The responses for a range of transmitter frequencies.. The three-layered disk burial depth is 525 m and the transmitter is located at XTX = -1000 m.

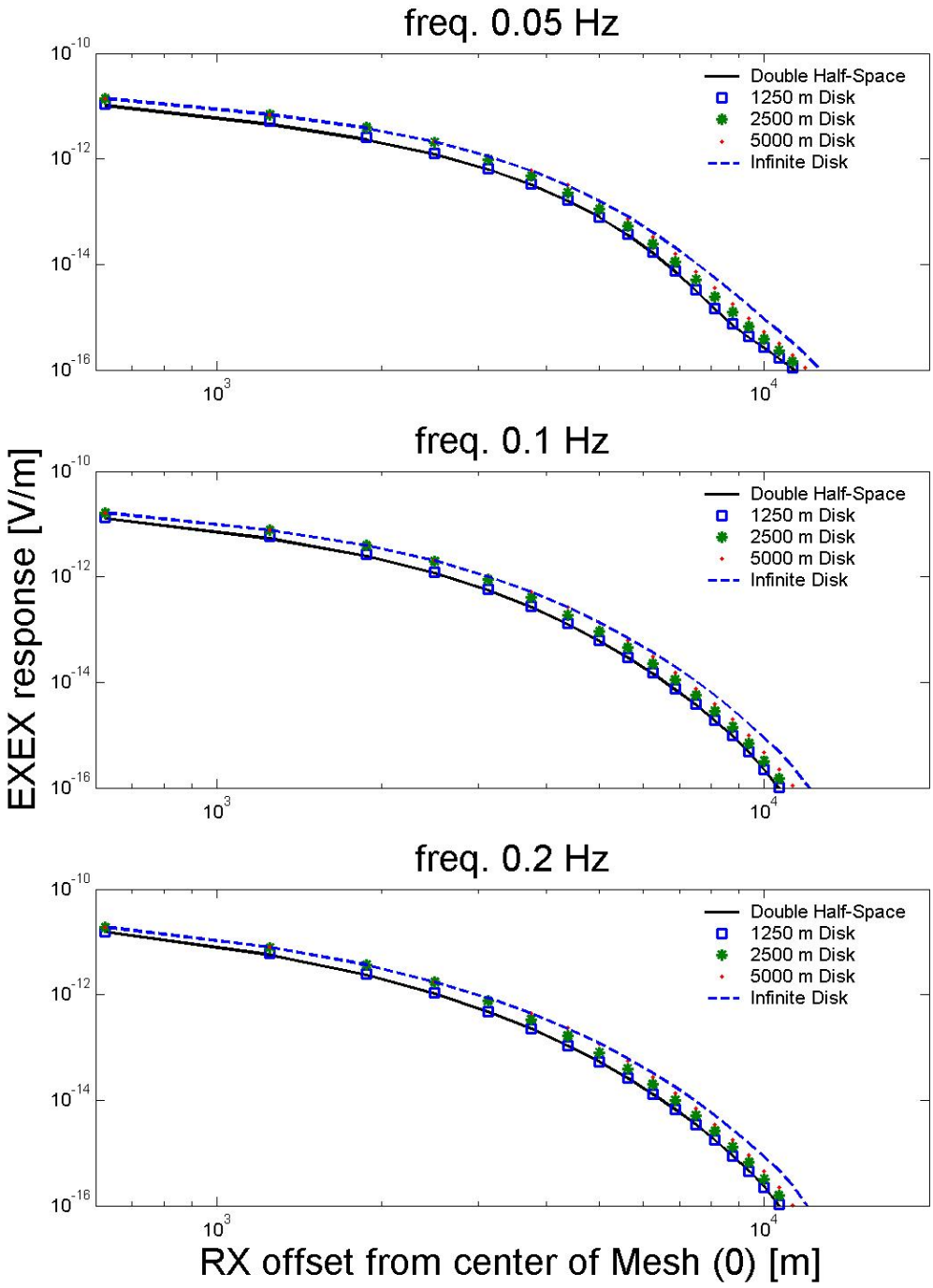

Figure 16 - The responses for a range of transmitter frequencies.. The three-layered disk burial depth is 525 m and the transmitter is located at XTX = -1000 m.

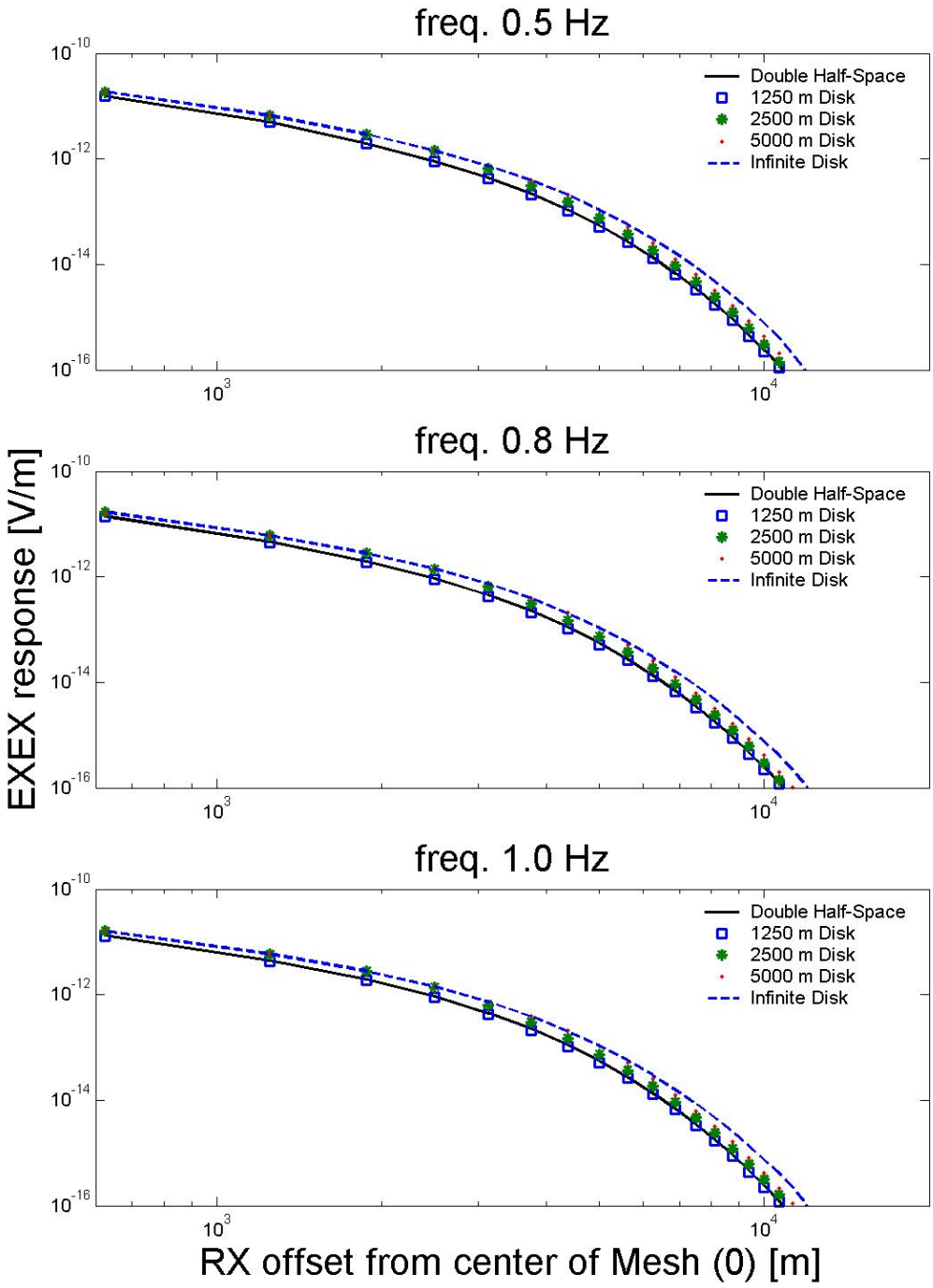

Figure 17 - The responses for a range of transmitter frequencies. The three-layered disk burial depth is 525 m and the transmitter is located at XTX = -1000 m.

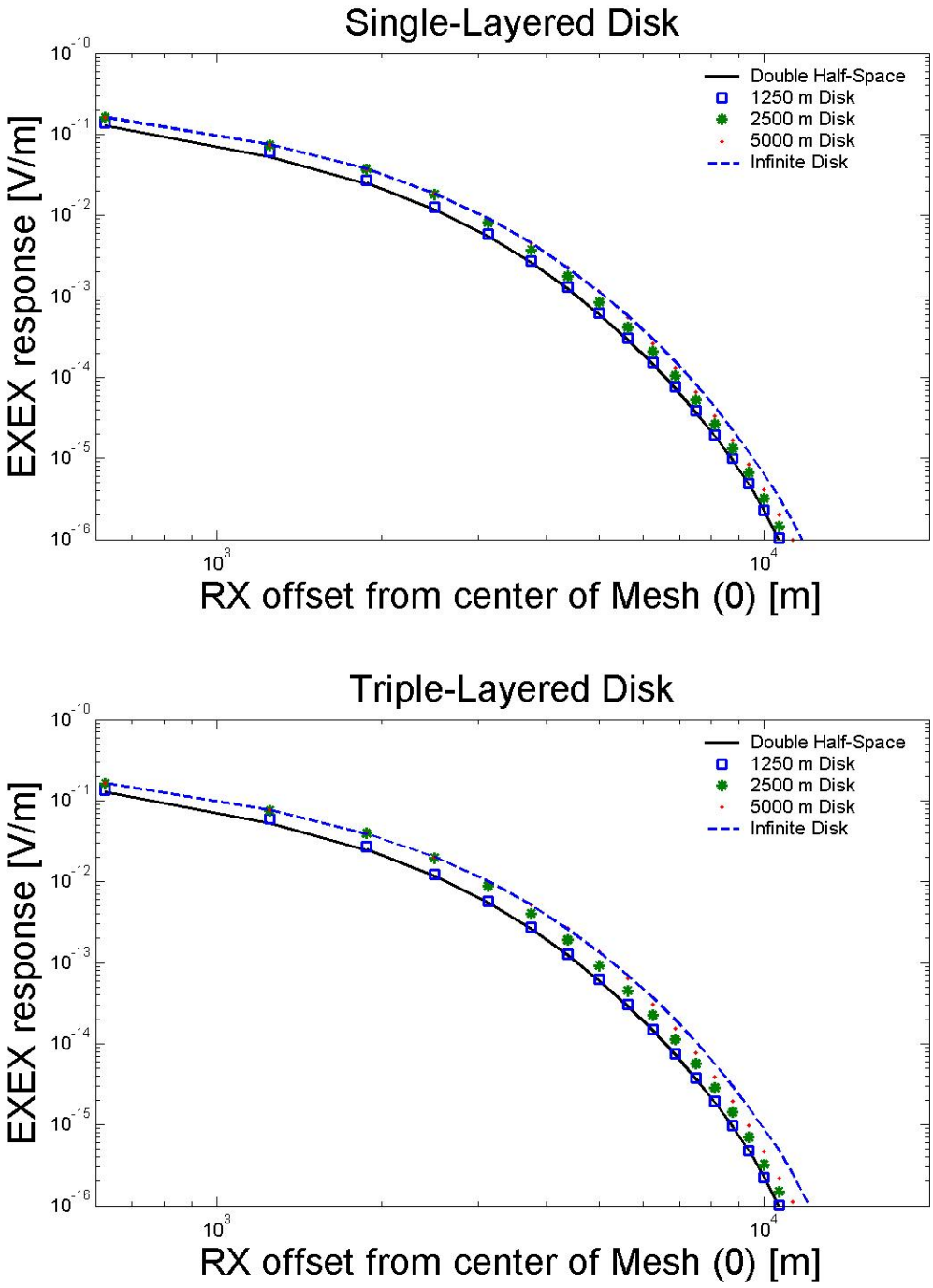

Figure 18 - The responses for a transmitter frequency of 0.1 Hz. The disk burial depths are 525 m and the transmitter is located at XTX = -1000 m.

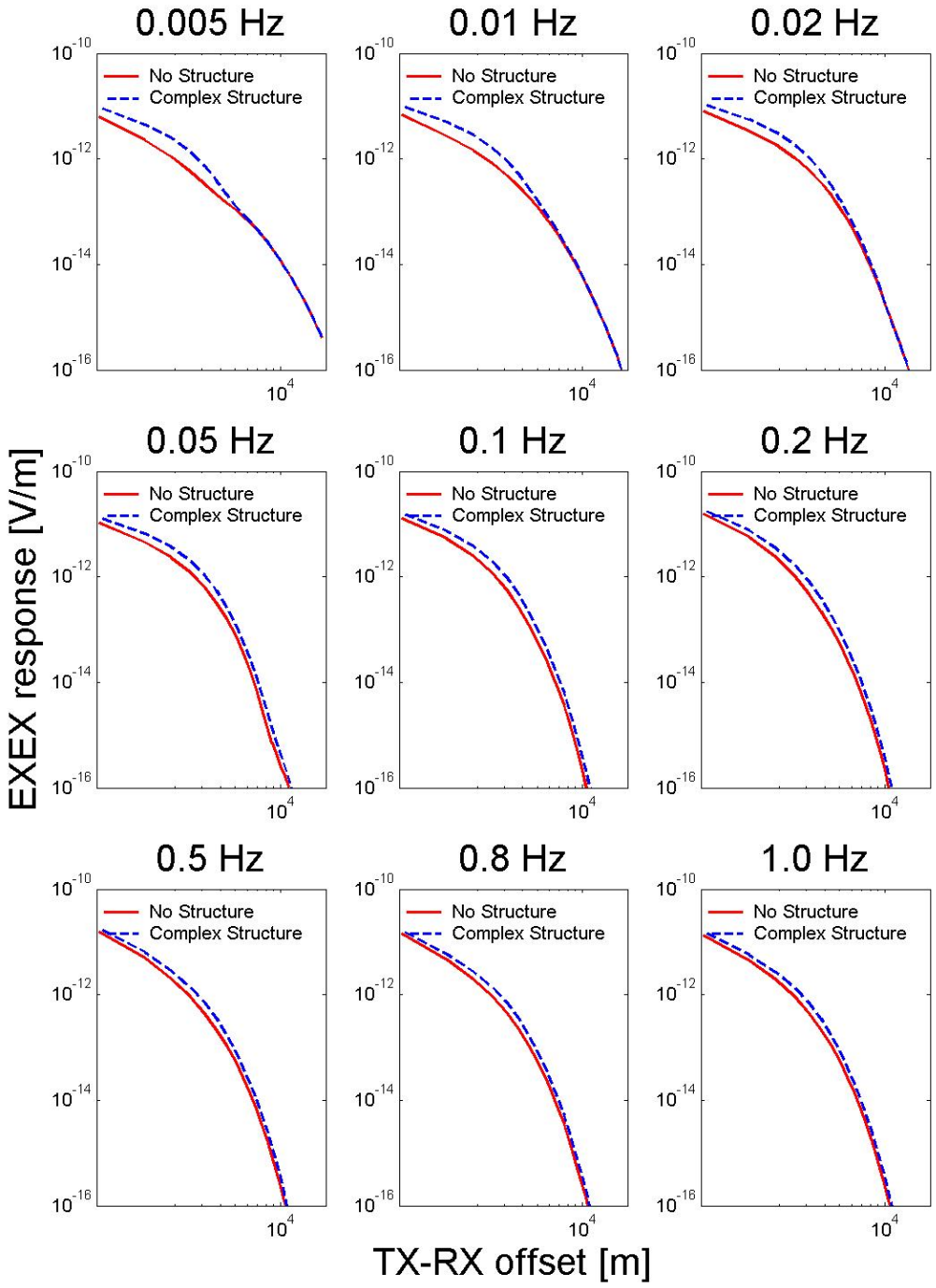

Figure 19 - The responses for a range of transmitter frequencies. The complex structure is buried at 525 m and the transmitter is located at XTX = -1000 m. The structure is open towards the negative side of the x-axis

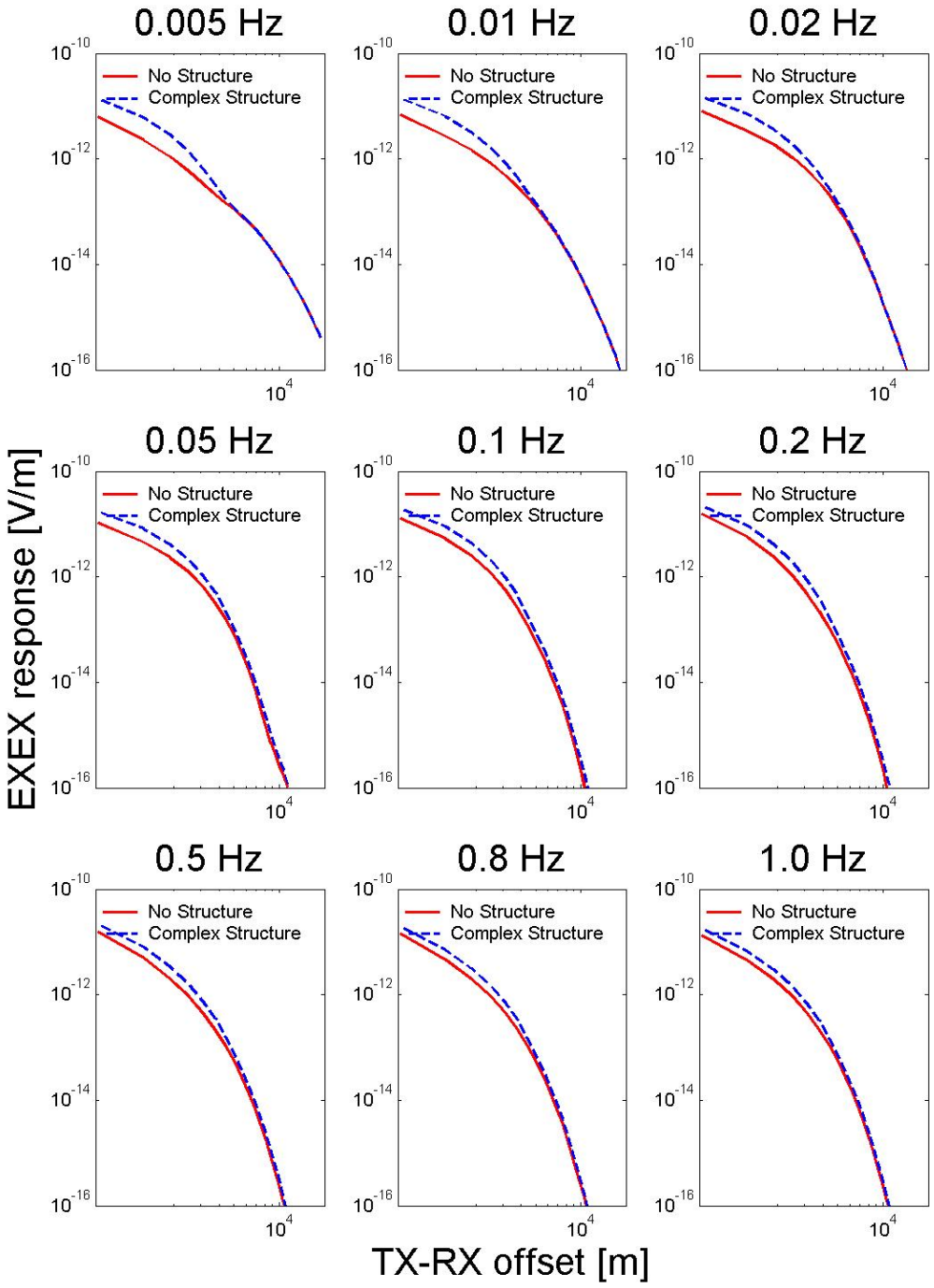

Figure 20 - The responses for a range of transmitter frequencies. The complex structure is buried at 225 m and the transmitter is located at XTX = -1000 m. The structure is open towards the negative side of the x-axis.

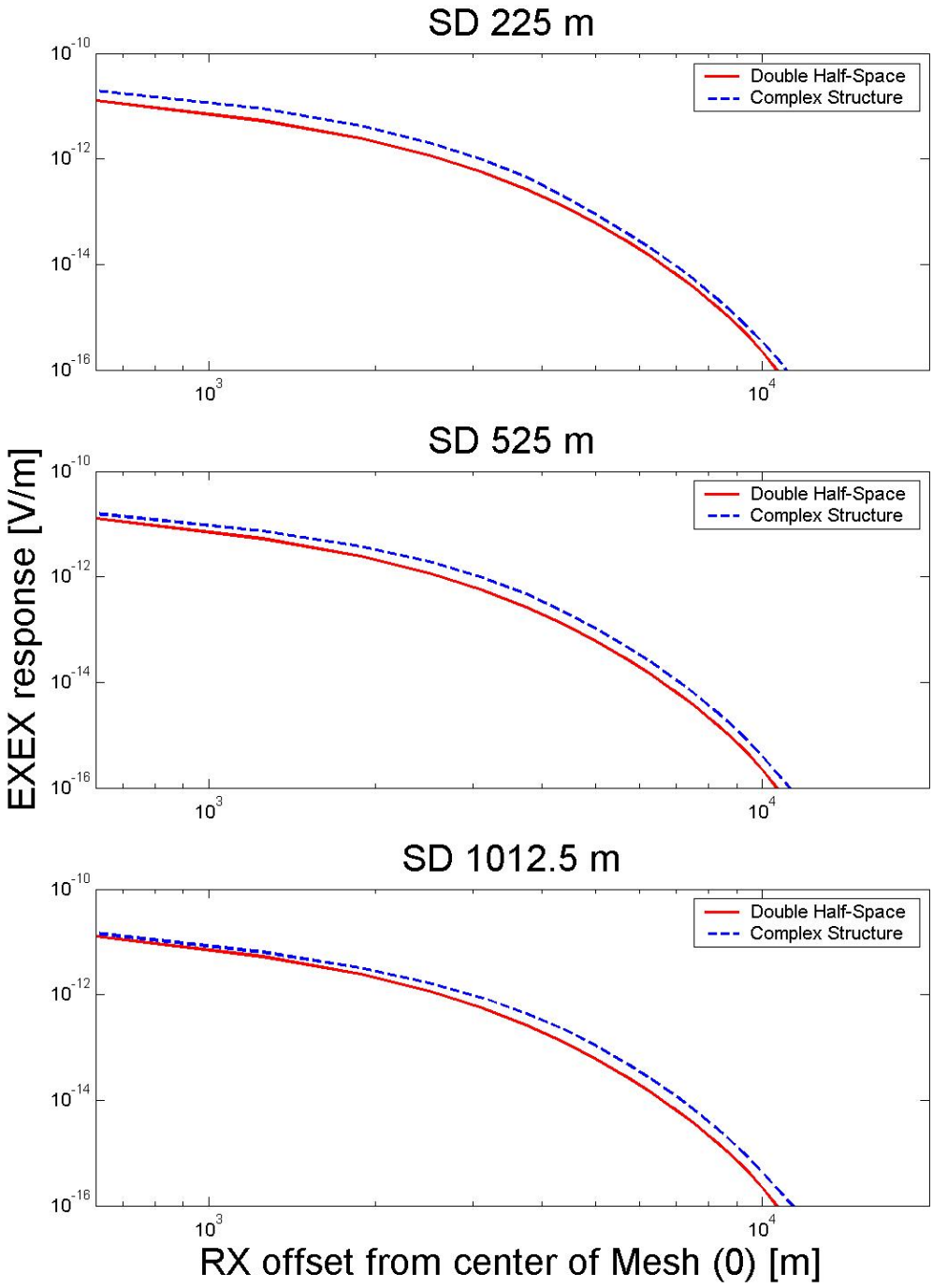

Figure 21 - A comparison of different burial depths for the complex geometric structure. The frequency is 0.1 Hz and the TX location is -1000 m.

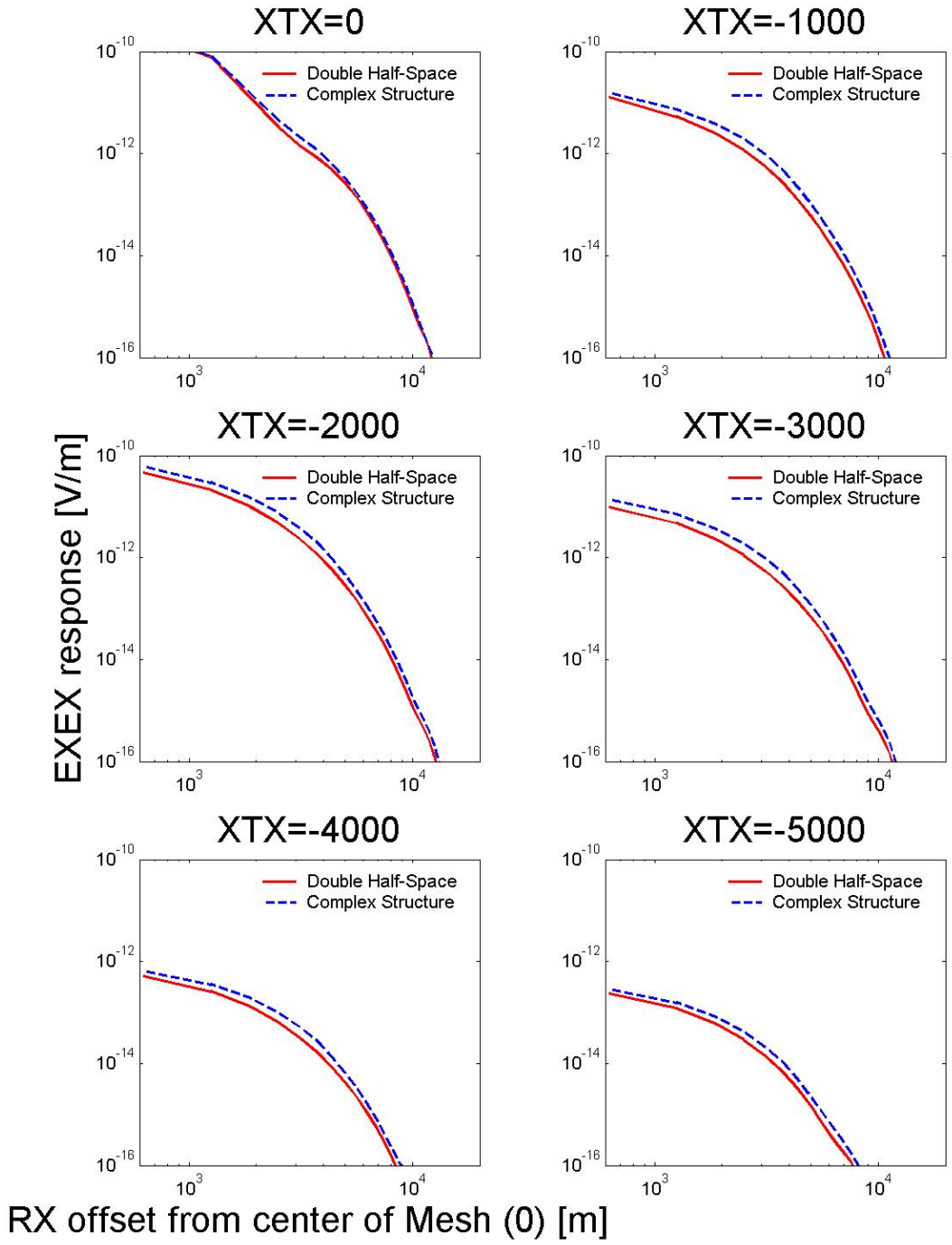

Figure 22 - The responses for a range of transmitter locations. The transmitter frequency is 0.1 Hz and the structure is buried at 525 m. The structures open end is facing towards the negative side of the x-axis. The structure is ~112 m thick.

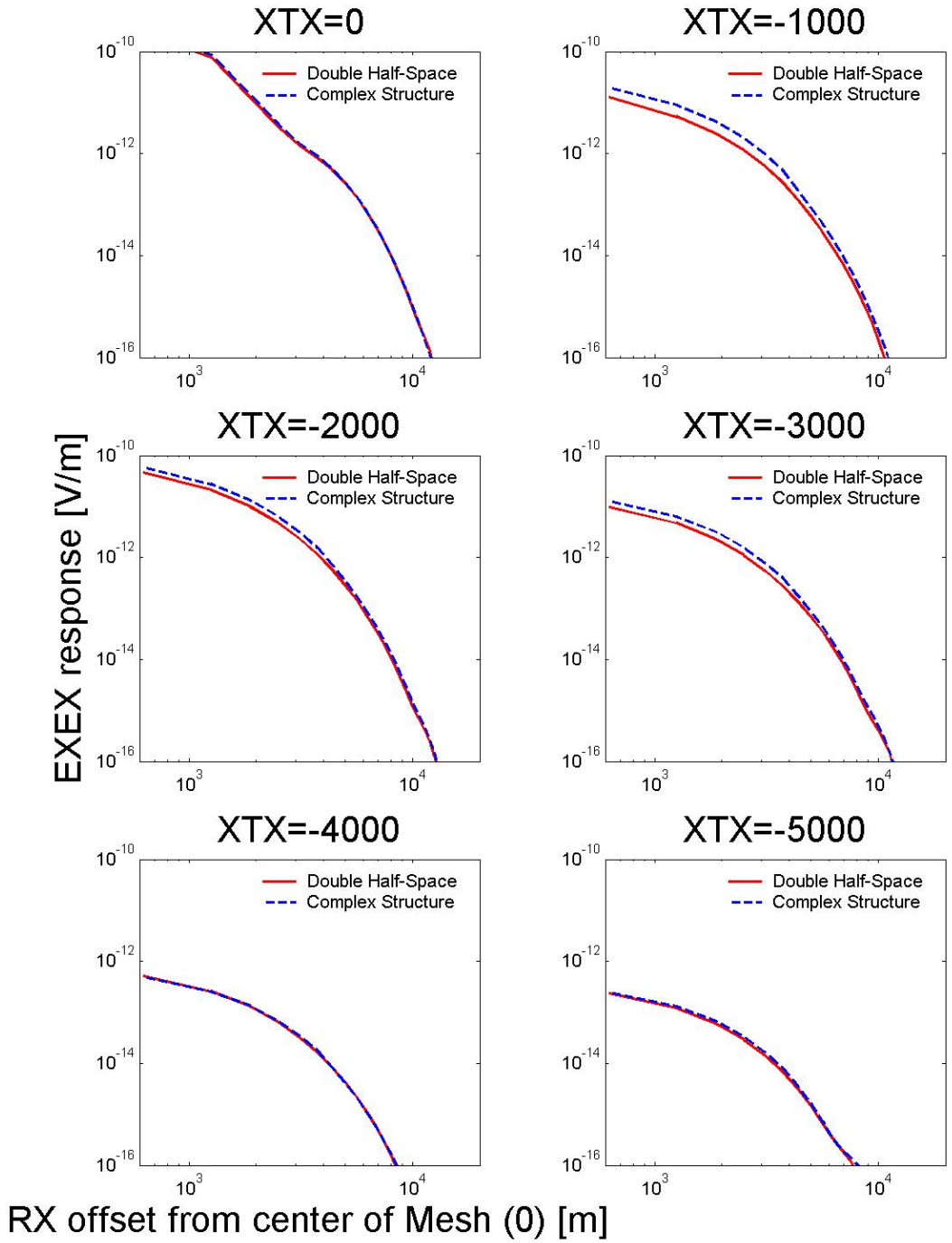

Figure 23 - The responses for a range of transmitter locations. The transmitter frequency is 0.1 Hz and the structure is buried at 225 m. The structures open end is facing towards the negative side of the x-axis. The structure is ~ 112 m thick.

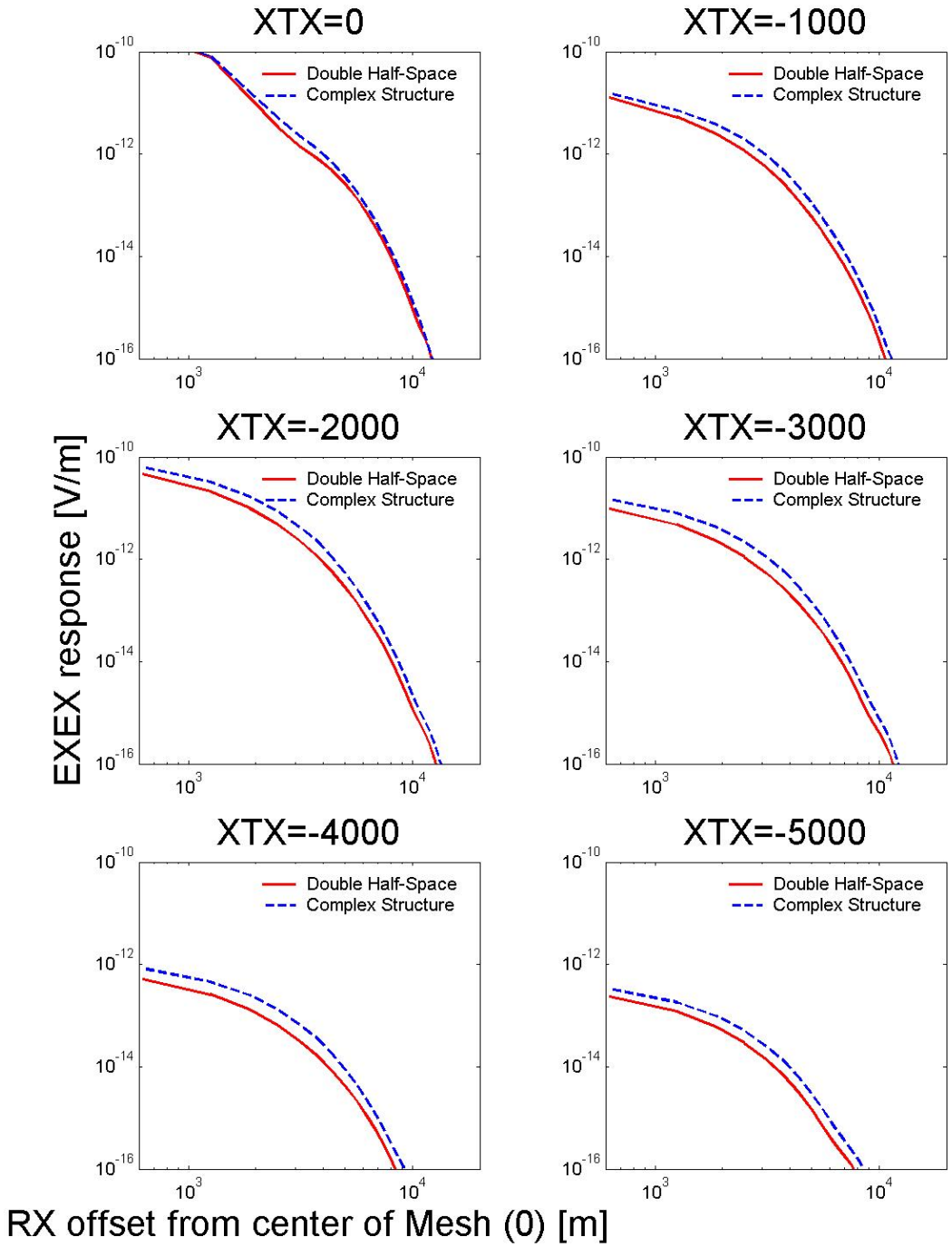

Figure 24 - The responses for a range of transmitter locations. The transmitter frequency is 0.1 Hz and the structure is buried at 525 m. The structures open end is facing towards the negative side of the x-axis. The structure is ~ 336 m in thickness.

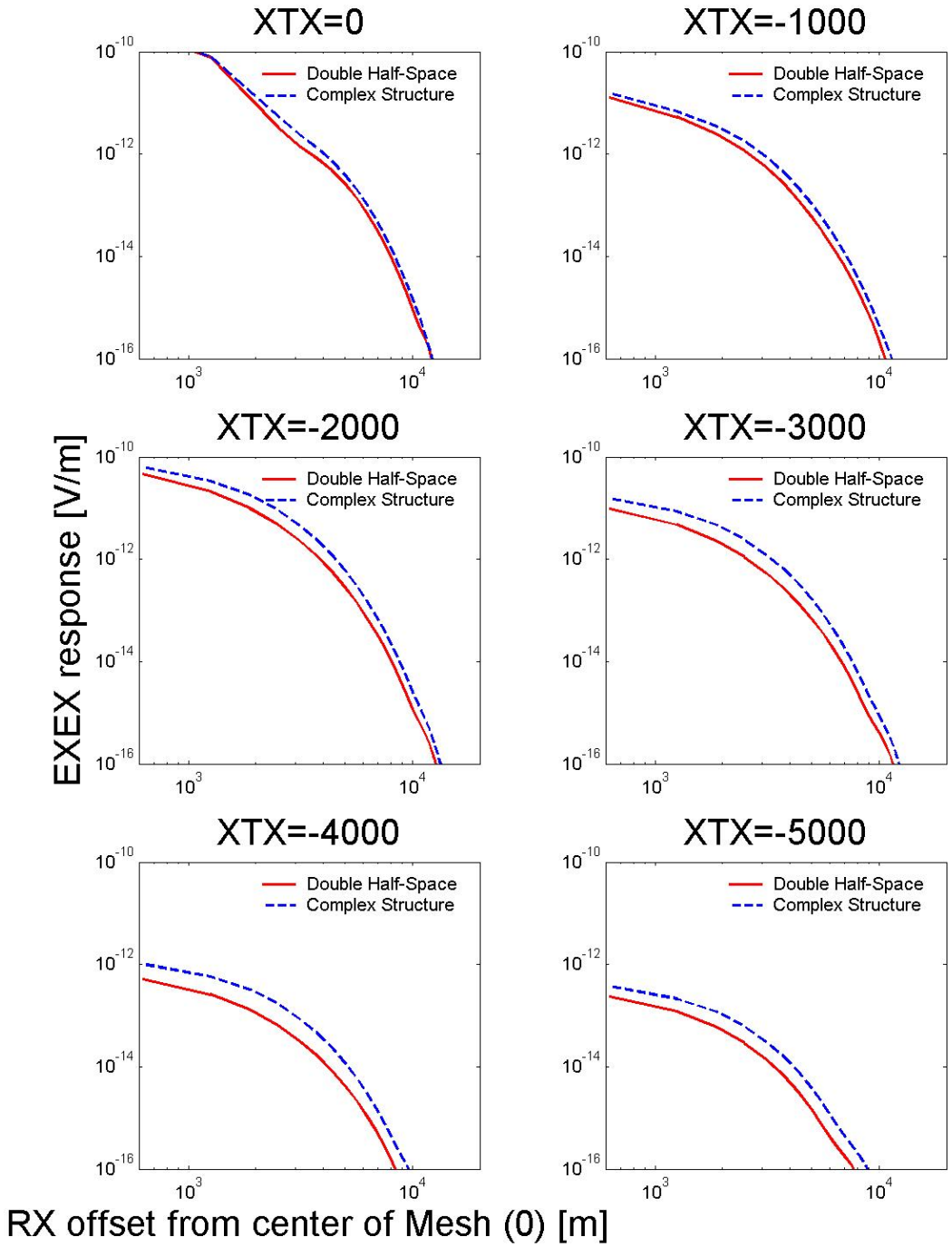

Figure 25 - The responses for a range of transmitter locations. The transmitter frequency is 0.1 Hz and the structure is buried at 525 m. The structure's open end is facing towards the negative side of the x-axis. The structure is ~ 675 m in thickness.

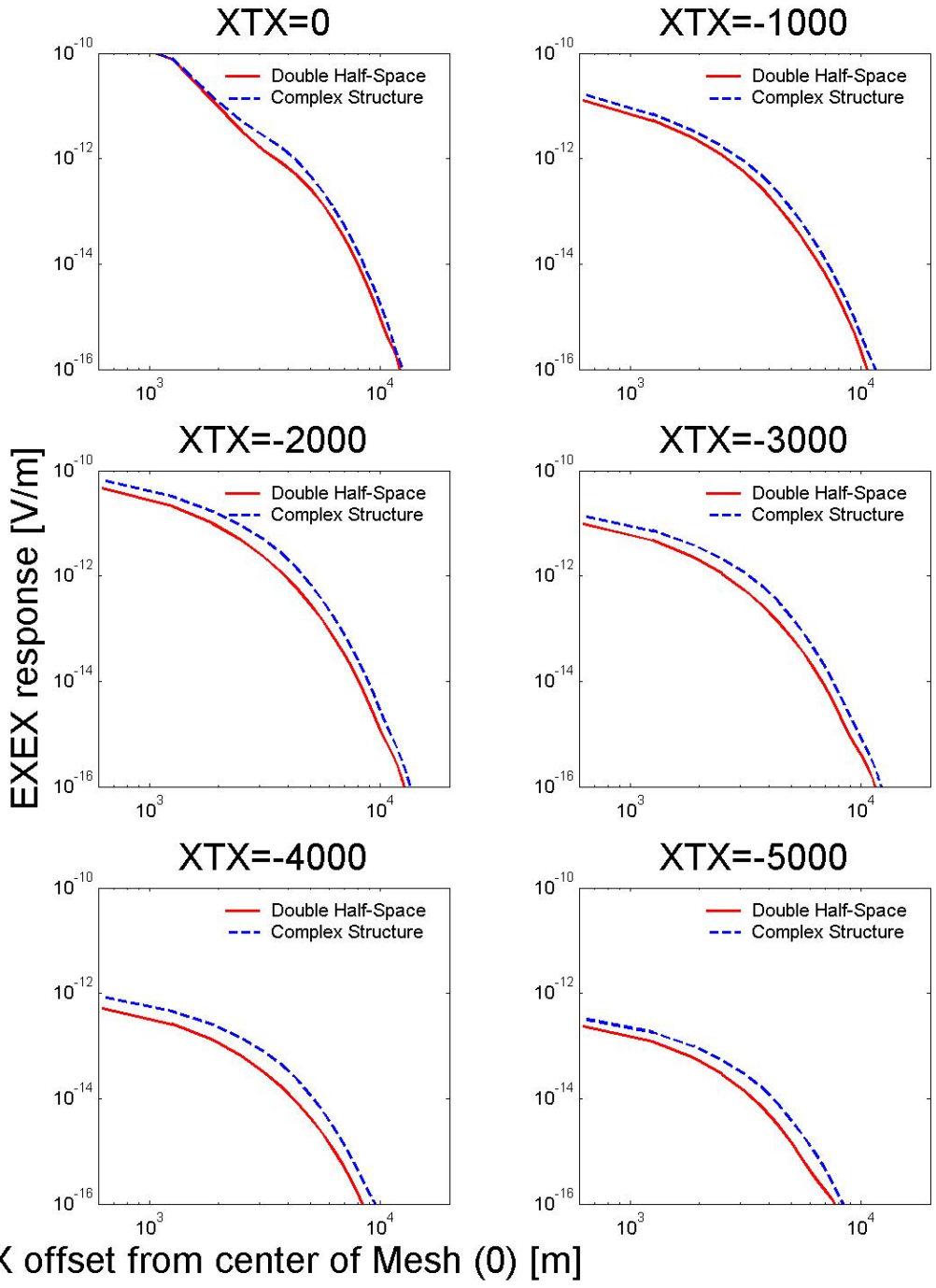

Figure 26 - The responses for a range of transmitter locations. The transmitter frequency is 0.1 Hz and the structure is buried at 525 m. The structure's open end is facing towards the positive side of the x-axis. The structure is ~ 675 m in thickness.

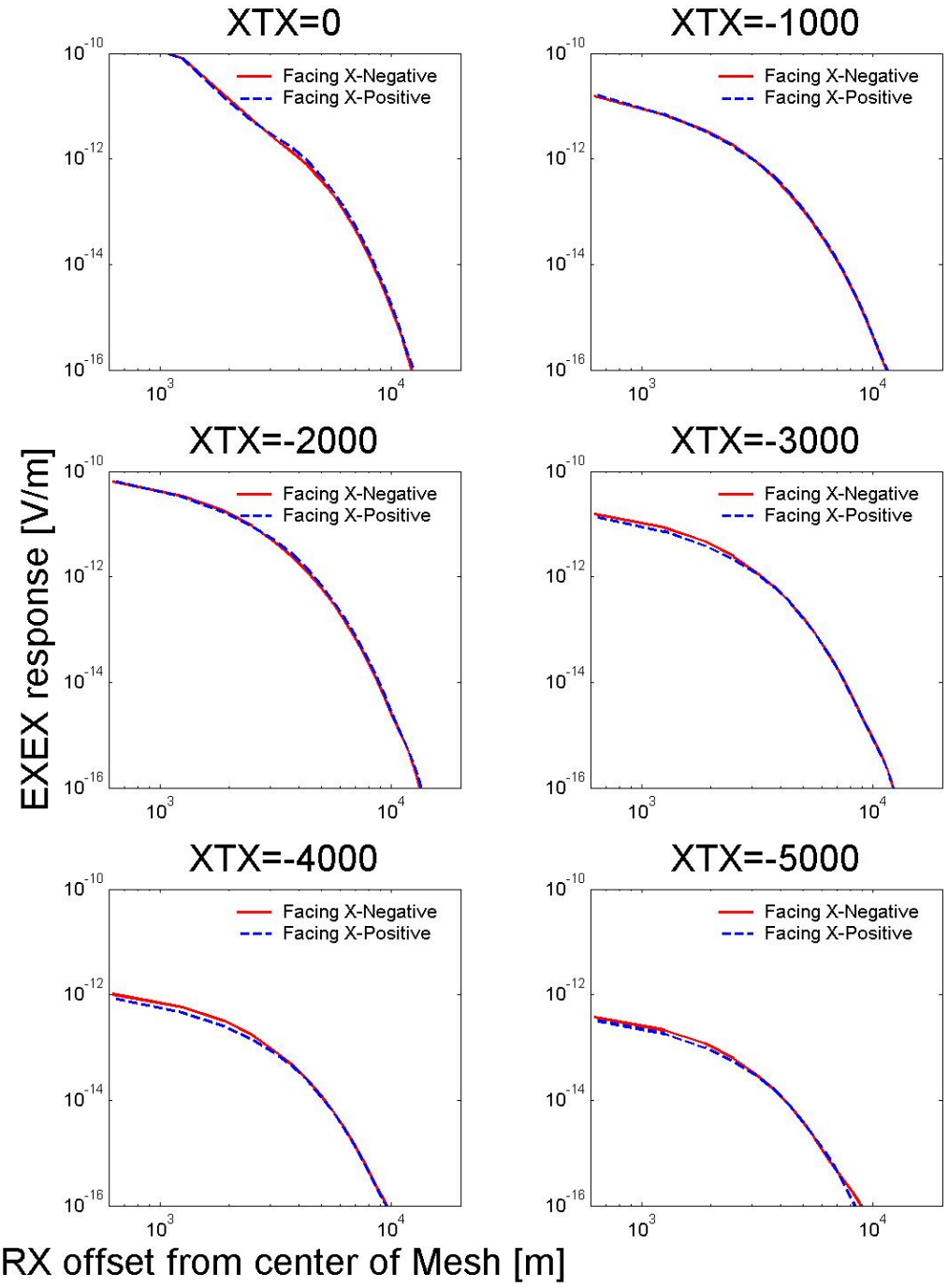

Figure 27 - Structure responses for two of the three orientations. The frequency is 0.1 Hz, depth of burial 525 m, and the thickness of the structure is about 675 m.

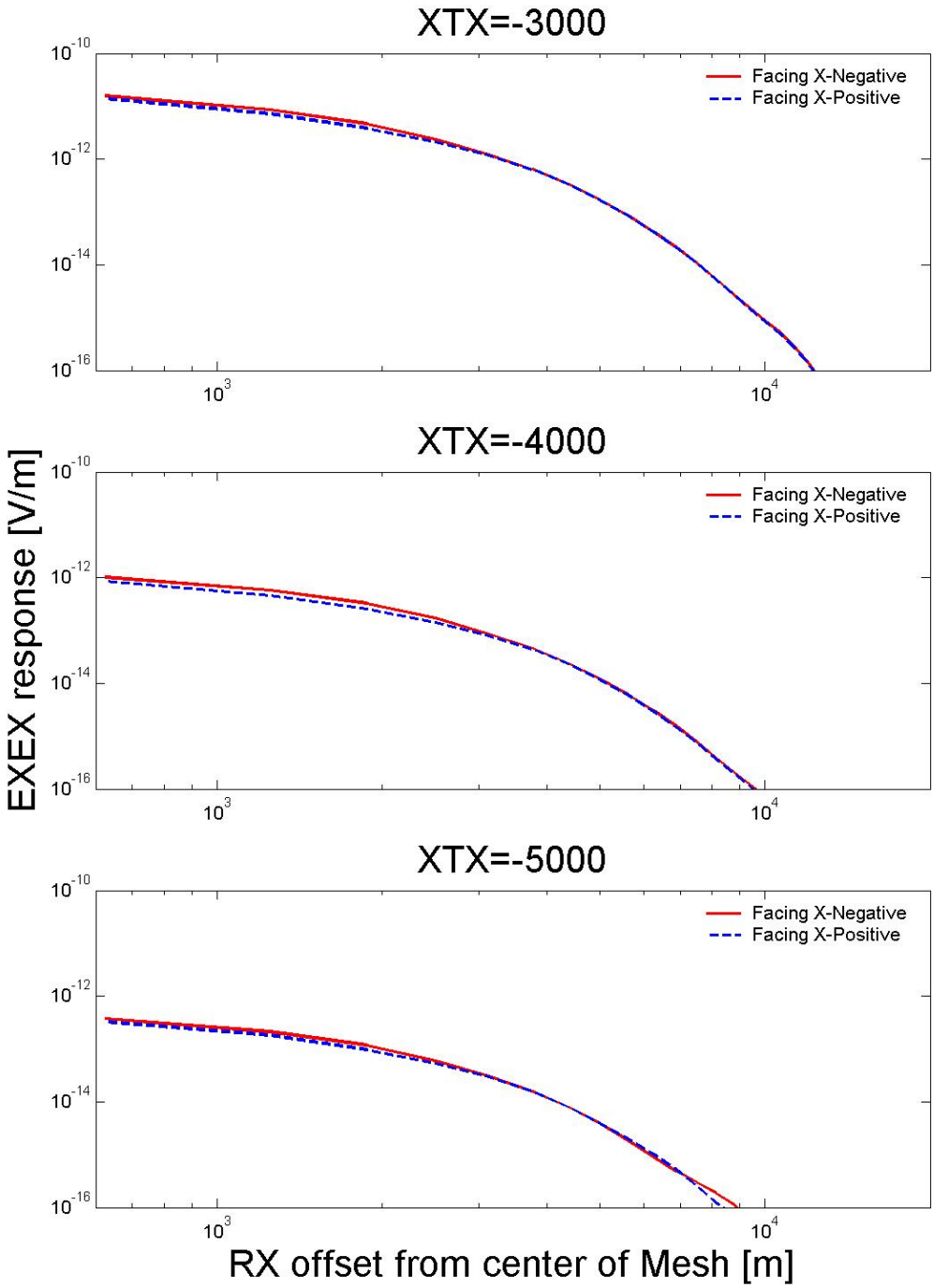

Figure 28 - Structure responses for two of the three orientations. The frequency is 0.1 Hz, depth of burial 525 m, and the thickness of the structure is about 675 m.

APPENDIX II: TABLES

Table 1 - An example of local refinement used for Fig. 4-7.

	Δr [m] radial extent		Δz [m] depth extent		ΔΦ [m] radial extent	
Refinement	min.	max.	min.	max.	min.	max.
1	0	1562.5	-840	840	-π	π
2	0	937.5	-560	560	-π	π
3	0	312.5	-280	280	-π	π
4	0	156.25	-140	140	-π	π

Table 2 - Shown are the skin depths for seawater and sediments

Frequency (Hz)	**Seawater (0.333 Ohm-m) skin depth (m)**	**Sediments (1.0 Ohm-m) skin depth (m)**
1.0	289	500
0.8	323	559
0.5	408	707
0.2	645	1118
0.1	912	1581
0.05	1290	2236
0.02	2040	3536
0.01	2885	5000
0.005	4080	7071

VITA

Joshua David King
459 Bakerville Road
Dartmouth, MA 02748

EDUCATION

Texas A&M University, College Station, TX
M.S. in geophysics, December 2004

Keene State College, Keene, NH
B.S. in geology, May 2001

EXPERIENCE

Summer 2003	GRADUATE RESEARCH ASSISTANT for Mark Everett at Texas A&M University, College Station, TX
September 2002-May 2004	GRADUATE TEACHING ASSISTANT for Dept. of Geology and Geophysics, Texas A&M University, College Station, TX
July 2002	STUDENT, Geophysics Field Camp, Summer of Applied Geophysics Experience, Santa Fe, NM
July 2001	STUDENT, Geology Field Camp, Indiana University at Bloomington, Caldwell, MT
2000-2002	GEOLOGICAL TECHNICIAN for Steven Brackett of Brackett Geosciences, Keene, NH
2000	GEOLOGICAL TECHNICIAN for SVE Associates, Keene, NH
1997-2001	STUDENT WORKER/STUDENT SUPERVISOR for Mason Library, Keene State College, Keene, NH